

Aboveground biomass of typical invasive mangroves and its distribution patterns using UAV-LiDAR data in a subtropical estuary: Maoling River estuary, Guangxi, China

Yichao Tian ^{a,b,c}, Qiang Zhang ^a, Hu Huang ^{b,*}, Youju Huang ^d, Jin Tao ^a, Guoqing Zhou ^e, Yali Zhang ^a, Yongwei Yang ^a, Junliang Lin ^a

^a School of Resources and Environment, Beibu Gulf University, Qinzhou 535011, China

^b Guangxi Key Laboratory of Marine Disaster in the Beibu Gulf, Beibu Gulf University, Qinzhou 535011, China

^c Key Laboratory of Marine Geographic Information Resources Development and Utilization in the Beibu Gulf, Beibu Gulf University, Qinzhou 535011, China

^d Guangxi Zhuang Autonomous Region Remote Sensing Institute of Natural Resources, Nanning 530023, China

^e Guangxi Key Laboratory for Geospatial Informatics and Geomatics Engineering, Guilin University of Technology, Guilin 541004, China



ARTICLE INFO

Keywords:

Machine learning algorithms
UAV-LiDAR
Aboveground biomass
Invasive mangroves
Hydrology and geomorphology
Beibu Gulf
Maoling river estuary

ABSTRACT

Quantitative assessment of aboveground biomass (AGB) and spatial distribution pattern of exotic mangrove plants (*Sonneratia apetala*) is of great significance for blue carbon management and ecological restoration in typical subtropical estuaries in China. Although unmanned aerial vehicle (UAV) light detection and ranging (LiDAR) has certain advantages in the investigation of the vertical three-dimensional structure of mangroves, the existing mangrove investigation results are mainly based on plot investigation method. Few scholars use machine learning (ML) method to estimate AGB of invasive *Sonneratia apetala* by combining plot investigation and LiDAR data. Therefore, on the basis of the height and intensity variables of UAV-LiDAR data, this study used four different ML algorithms, namely, **xgboost regressor (XGBR)**, **catboost regressor (CBR)**, **light gradient boosting regressor (LGBR)** and **AdaBoost regressor (ABR)**, to estimate AGB of invasive mangrove. Then, the quantitative relationship between invasive mangrove biomass and hydrological unit was analysed. We found that CBR model had the highest accuracy in estimation of mangrove AGB ($R^2 = 0.7644$, RMSE = 11.1725 Mg/ha), followed by XGBR model ($R^2 = 0.6759$, 13.1053 Mg/ha). However, LGBR model ($R^2 = 0.3506$, RMSE = 18.5510 Mg/ha) had poor fitting effect. The AGB of invasive mangroves showed a spatial distribution pattern of high in northwest and low in southeast, and its value ranged from 7.31 Mg/ha to 114.04 Mg/ha, with an average of 25.57 Mg/ha. The AGB of invasive mangroves was independent of the area size of the hydrological response unit but depended on the elevation of the beach surface and the distance from the main tidal ditch. This study demonstrates the feasibility of UAV-LiDAR remote sensing and CBR model in estimating AGB of invasive mangrove species, which can provide scientific basis and technical support for the assessment of invasive mangrove ecosystem and the protection of local mangrove tree species.

1. Introduction

Mangrove is a woody biological community composed of evergreen shrubs or trees with mangrove plants as the main body, and it grows in the upper intertidal zone of tropical and subtropical coasts and is flooded by periodic tides. It is an important feeding place for some fish, birds, and marine mammals. It has the functions of promoting siltation and land building, wave protection, maintaining biodiversity, and

resisting natural disasters and a series of ecosystem service functions (Murdiyarno et al., 2015; Mumby et al., 2004; Trégarot et al., 2021; Hu et al., 2020; Zhu et al., 2021; Xia et al., 2021; MacDonnell et al., 2017). In addition, mangrove ecosystems have a strong carbon sink capacity, which is important for mitigating global climate change (Alongi, 2014; Liu et al., 2014). Blue carbon ecosystem refers to the ecosystem composed of coastal higher plants such as salt marsh wetland, mangrove and seagrass bed, as well as phytoplankton, algae and shellfish. Under

* Corresponding author at: Guangxi Key Laboratory of Marine Disaster in the Beibu Gulf, Beibu Gulf University, No.12, Binhai Avenue, Qinzhou, Guangxi, China (H. Huang).

E-mail addresses: tianyichao1314@hotmail.com (Y. Tian), mrhuanghu@126.com (H. Huang).

the joint action of their own growth and microorganisms, CO₂ in the atmosphere is absorbed, transformed and preserved in the sediment of the coastal zone for a long time, and part of the organic carbon exported from coastal zone to offshore and ocean (Zhang et al., 2015; Howard et al., 2017; Mcleod et al., 2011). These three types of ecosystems account for only 0.2% of the global ocean area, but the carbon sequestration capacity per unit area of these three types of ecosystems is 10 times that of terrestrial ecosystems (Mcleod et al., 2011). Mangroves account for only 0.1% of the global land area, but their carbon sequestration accounts for 5% of the global total carbon sequestration (Bouillon et al., 2008). Carbon sequestration by mangrove vegetation and sediments is approximately three to four times higher than that of tropical rain forests (Yees, 2010). Mangrove aboveground biomass (AGB), as an important part of coastal blue carbon ecosystems, plays an important role in mitigating and coping with climate change (Mcleod et al., 2011; Luo and Chui, 2020). AGB is the basis for studying vegetation carbon storage. Estimation of mangrove AGB can provide an important reference for the study of wetland carbon sinks. Therefore, quantitatively evaluating the AGB of mangrove wetlands and fully tapping and maintaining and enhancing the carbon sink potential of mangroves has great theoretical and practical importance to achieve China's goal of 2030 peaking carbon dioxide emissions and vision of 2060 carbon neutrality. At the same time, the assessment of AGB and blue carbon of mangroves can help China achieve carbon peak by 2030 and carbon neutralization by 2060 as soon as possible, which is also a major strategic decision made by China to achieve the goal of addressing climate change.

Sonneratia apetala is an excellent fast-growing tree species of mangroves, and it is naturally distributed in India, Bangladesh, Sri Lanka, and other countries (Hu and Zhao, 2005). In 1985, China went to Bangladesh and brought back *Sonneratia apetala* fruit, which was successfully cultivated in Dongzhai Port, Hainan. In 2001, *Sonneratia apetala* was introduced from Zhanjiang in Qinzhou, Guangxi, and large-scale afforestation was conducted along the coast. At present, *Sonneratia apetala* can achieve natural regeneration in the Kangxiling area of Qinzhou, Guangxi, and it can quickly occupy suitable forest land and even invade the original mangrove community. It shows a certain invasiveness in the coastal area of Beibu Gulf, Guangxi, and it has a certain impact on the coastal mangrove ecosystem (Deng, 2020). With the global warming, *Sonneratia apetala* has spread in the coastal beaches of Qinzhou City in the Beibu Gulf by relying on its strong breeding ability and rapid growth ability. Due to the rapid growth of its trunk and luxuriant branches, the invaded *Sonneratia apetala* immediately occupies the upper nutritional space, and the native mangrove plants become the lower vegetation. The photosynthesis is limited, and the accumulation of biomass is reduced, which will affect the normal physiological activities of native mangrove plants, and then change the ecosystem structure and function of native mangrove plants, endangering the survival and growth of native species (Tang et al., 2012). In addition, the growing place of *Sonneratia apetala* will also lead to serious rat and snake diseases. The reason may be that a large number of fruits of *Sonneratia apetala* attract mice to eat, and snakes eat mice, forming a food chain of "Sonneratia apetala-mouse-snake". We can understand the growth status, structural development degree, and stress level of the invasive mangrove system on the native *Aegiceras corniculata* species by evaluating the productivity and aboveground biomass of the invasive mangrove (Soares and Schaeffer-Novelli, 2005). However, field investigation of mangrove biomass is difficult because of the special habitat conditions of the coastal intertidal zone and the complexity of the mangrove ecosystem structure. Field surveys are a basic and accurate method for obtaining mangrove community parameters. A mangrove field survey has several advantages. However, the monitoring of mangrove population by using the traditional quadrangle survey method will be greatly affected by adverse natural conditions such as the silt on the shoal and tidal fluctuation because of the restriction by the growth conditions of the intertidal zone between sea and land due to the

muddy shoal of mangroves. This situation greatly increases the costs of manpower, financial resources, and time (Gao, 1999). Remote sensing technology has significant advantages in mangrove monitoring because of its wide field of vision, large amount of information, high efficiency, and strong adaptability. It has become one of the main technologies for mangrove research at home and abroad (Navarro et al., 2019; Hamdan et al., 2014; Guo et al., 2021; Ibiharim et al., 2015; Jayanthi et al., 2018; Kovacs et al., 2008; Le et al., 2020; Liao et al., 2019).

Remote sensing technology has the advantages of large-scale monitoring, short cycle, sustainability, large amount of information, and high cost performance. Applying remote sensing technology to mangrove monitoring can achieve comprehensive, rapid, dynamic, and accurate mangrove monitoring (Soares and Schaeffer-Novelli, 2005). At present, three common remote sensing technologies can be used to estimate the aboveground biomass of mangroves: passive optical remote sensing, radar remote sensing, and LiDAR remote sensing (Wang et al., 2019a; Wang et al., 2019b). Passive optical remote sensing is the earliest and most commonly used mangrove biomass mapping method for estimating mangrove AGB. This method has wide data coverage and easy access. Many studies have used optical satellite remote sensing technology to evaluate the mangroves AGB in different regions, and several gratifying results have been obtained. Most scholars use MODIS data of low resolution (Lu, 2006) and remote sensing data of moderate spatial resolution, such as Landsat TM/ETM+/OLI and ASTER, to invert mangrove AGB at a large regional scale (Pham et al., 2019; Hickey et al., 2018; Cao et al., 2010; Jachowski et al., 2013). Some scholars use QuickBird, IKONOS, WorldView-2, RapidEye, and other high-resolution optical data to estimate the biomass of mangroves at a small scale, and their research results proved that high-resolution satellite data can significantly improve the accuracy of mangrove AGB estimation (Cahyaningrum et al., 2014; Phua et al., 2014; Manna et al., 2014; Zhu et al., 2015; Hirata et al., 2014). However, low-and medium-resolution data are easily affected by satellite mixed pixels, which limits their wider application. In the meantime, the popularisation of high-resolution data on a large scale is limited owing to their high cost. Active radar remote sensing satellite data such as dual-pol SAR (Vaghela et al., 2021), ALOS PALSAR (Castillo et al., 2017), and Sentinel-1C-band SAR are vulnerable to saturation effects. In addition, passive optical remote sensing and radar remote sensing cannot monitor the complete vertical canopy information in vegetation areas with high biomass because optical remote sensing only obtains canopy surface information, while the penetration ability of radar is limited (Wang et al., 2019a; Wang et al., 2019b).

UAV-LiDAR is an advanced active remote sensing technology. It uses unmanned aerial vehicles (UAV) as a platform and carries light detection and ranging (LiDAR) sensors to obtain three-dimensional information of ground objects (Dalla Corte et al., 2020). UAV-LiDAR has a stronger mobility and lower cost than traditional optical remote sensing. It is suitable for the collection of three-dimensional ground object information, such as mangroves. Over the past two decades, manned LiDAR data have played a significant role in the estimation of forest AGB (García et al., 2010). However, the acquisition cost of manned LiDAR data is usually very high, and the development and application of these data in forestry are limited to a certain extent owing to factors such as mission safety and flight conditions (Guo et al., 2017; Shi et al., 2018). With the rapid development of UAV hardware and portable LiDAR sensors in recent years, UAV-LiDAR has been gradually used in mangrove AGB estimation. For example, Wang et al. (2019a); Wang et al. (2019b) and Qiu et al. (2019) used the random forest (RF) method to estimate the AGB of mangroves in different areas of Hainan Island based on UAV-LiDAR remote sensing data and sample plot measured data. Salum et al. (2020) estimated the AGB of mangroves on Guaras Island using a linear equation based on tree height data derived from UAV-LiDAR and the measured sample plot data. From the existing research results, the application of UAV-LiDAR in mangrove AGB mainly involves two categories: parametric regression models (Salum et al., 2020) and nonparametric machine learning methods (Wang et al., 2019a; Wang

et al., 2019b; Qiu et al., 2019). The parametric regression model method is based on the hypothetical relationship between biomass and predictors. The model assumes that a simple linear relationship exists between the predictive variables and biomass. However, this assumption cannot generate satisfactory results when estimating forest AGB (Pandit et al., 2018). Nonparametric machine learning methods such as RF, support vector machine (SVM), and Kohonen neural network can deal with nonlinear relationships. These methods can determine the key driving factors affecting forest biomass from complex predictors to realise the quantitative estimation of biomass (Zhao et al., 2019; Peng et al., 2019). These methods have been successfully applied to the study of mangrove AGB (Wu et al., 2016; Pham et al., 2018; Jachowski et al., 2013).

UAV laser remote sensing data can derive a large number of height and intensity variables. Extracting dominant features has become a key problem in improving the accuracy of mangrove species biomass estimation. Traditionally, many data dimensionality reduction or feature extraction methods are available, such as principal component analysis, independent component analysis, minimum noise separation (Xia et al., 2014), and continuous projection algorithms (Xu et al., 2019). These methods do not have a prediction function and need to be combined with other parametric regression methods to estimate the forest biomass. A new machine learning method gradient boosting algorithm, which has the functions of feature selection and prediction, is introduced in this study to improve the accuracy and efficiency of mangrove AGB. This algorithm is an integrated learning algorithm based on boosting strategy, and it mainly focuses on reducing the deviation and continuously improving the performance by learning multiple base learners in turn (Song et al., 2020; Chen and Guestrin, 2016). In this study, four kinds of gradient lifting algorithms are mainly used, namely, xgboost regressor (XGBR) (Tian et al., 2021), catboost regressor (CBR) (Zhou et al., 2021), light gradient boosting regressor (LGBR) (Jian et al., 2019) and AdaBoost regressor (ABR) algorithms (Jian et al., 2019). Gradient lifting has better prediction performance than other commonly used machine learning methods (e.g. Support Vector Machine(SVM) and Random Forest(RF)), and it is not easily affected by the quality of the training data.

The Kangxiling Mangrove Nature Reserve, as the northernmost mangrove distribution area of the Beibu Gulf, is a typical south subtropical estuary, harbour, and coastal beach wetland complex ecosystem reserve in China. The mangroves in this area are the planting areas of exotic *Sonneratia apetala* mangrove plants. In recent years, *Sonneratia apetala* on the coastal beach of Tuanhe Island has spread naturally over a large area, and this phenomenon has a certain impact on the growth space of local *Aegiceras corniculata*. However, research on the biomass estimation of *Sonneratia apetala* in the diffusion area is rare and scarce. Although UAV-LiDAR has certain advantages in the investigation of the vertical three-dimensional structure of mangroves, the existing mangrove investigation results in this area are mainly based on the plot investigation method. Few scholars have used machine learning methods to estimate the AGB of invasive *Sonneratia apetala* by combining the measured and laser LiDAR data. This study aims to use four new machine learning algorithms to evaluate the accuracy of different algorithms for the estimation of invasive mangrove AGB. On this basis, the optimal variables and machine learning models are selected to estimate the invasive mangrove AGB in the study area. This paper mainly has two research objectives. One is to quantitatively evaluate the accuracy and effect of AGB estimation of invasive mangroves by using four ML algorithms: XGBR, GBR, LGBR and ABR. The estimation of AGB in the study area is based on the optimization of different laser point cloud variables, and then the optimal ML algorithm is used to estimate the aboveground biomass of invasive mangrove. The second one is to find out what factors affect the spatial distribution pattern of mangrove AGB. The main content of this part is to extract the hydrological response unit, beach surface elevation and the spatial distribution of tidal ditch respectively through the digital elevation model

data generated by laser point cloud with the support of GIS software, and reveal the quantitative relationship between the AGB of invasive mangrove and hydrological response unit, beach elevation and tidal ditch through spatial statistical analysis. The purpose is to reveal the influencing factors of small-scale mangrove biomass spatial distribution pattern. The results of this study can provide a scientific basis and technical support for the evaluation of invasive mangrove ecosystems and the protection of local mangrove species.

2. Materials and methods

2.1. Study area

The MaoWeihai mangrove reserve is located in Qinzhou City, Beibu Gulf, Guangxi. It is mainly divided into four areas: Kangxiling (Maoling River Estuary), Jianxinwei, Seventy Jing, and Dafengjiang. The reserve has 11 families and 16 species of mangrove plants (including semi-mangrove and semi-mangrove plants) and 444 species of animals. Mangrove plants in the reserve account for 43.2% of the mangrove plants in China and 69.6% of the mangrove plants in Guangxi. The mangrove sample area in this study is located in the northwest of the Maowei Sea in Guangxi. The mangroves in this area are located in the Mangrove Nature Reserve in the Kangxiling area of the Maowei Sea. Rivers enter the sea in the Maoling River Basin in the northwest and Maowei Sea in Qinzhou Bay in the southeast. *Sonneratia apetala* in this area is spread from the mangrove species of artificial *Sonneratia apetala* in the north, and it has now been widely spread to the bund area of Tuanhe Island. Our Study area is carried out in Maoling River Estuary, Guangxi, China ($21^{\circ}51'7''$ N- $38^{\circ}51'47''$ N, $108^{\circ}29'4''$ E- $108^{\circ}30'20''$ E). The terrain of the study area is generally flat, with an area of $721\ 031.73\ m^2$. This area has a subtropical monsoon climate. It is located in a monsoon area in Southeast Asia. Solar radiation is strong, and the monsoon circulation is obvious (Tian et al., 2021). The annual average temperature is 21.7°C , the average precipitation is 1658 mm, the total annual sunshine hours are 1400–1950 h, and the average sunshine hours are 1673 h (Tian et al., 2019). Compared with the same period of the year, the sunshine hours are less, about 60 to 110 h. On the seasonal scale, the sunshine hours in winter and spring are more than those in the same period of the year, while those in summer and autumn are less than those in the same period of the year. The sunshine hours in different months show that the sunshine hours in January, February, April, June and October are more, while the sunshine hours in other months are less. The main river flowing into the Maowei Sea in the study area is the Maoling River. Most inland groups and islands are steamed, bread-shaped, low hills and flat terrain. In addition to the interaction of river and sea water, muddy flat beaches and tidal ditch island landscapes are formed at the entrance of the Maowei Sea, forming a typical sea fork terrain. The marine area of the Maowei Sea is rich in resources and shallow in water depth. Tidal flats account for approximately 80% of the total area of the bay, which is conducive to the deposition of sediment into the sea and the formation of soil conditions for the development of mangroves. The water temperature in the study area ranges from 16.2°C to 31.2°C , and the salinity ranges from 1.528 to 28.161 (Fig. 1).

2.2. Materials

2.2.1. Plot survey

In this study, the spread of *Sonneratia apetala* species in the Kangxiling area of Maowei Sea, Guangxi was selected for the sample plot investigation. Fig. 2(a) shows that the artificially planted *Sonneratia apetala* community spreads from the north to the bund area of Tuanhe Island in the south. Considering the interaction between the seawater of the Maowei Sea and the rivers flowing into the sea, *Sonneratia apetala* seeds spread along the tidal gullies (Fig. 2②) and propagated and grew locally in the Tuanhe Island bund area (Fig. 2③④⑤⑥). From January 20 to 23, 2021, after the tide receded, the teacher of our team led the

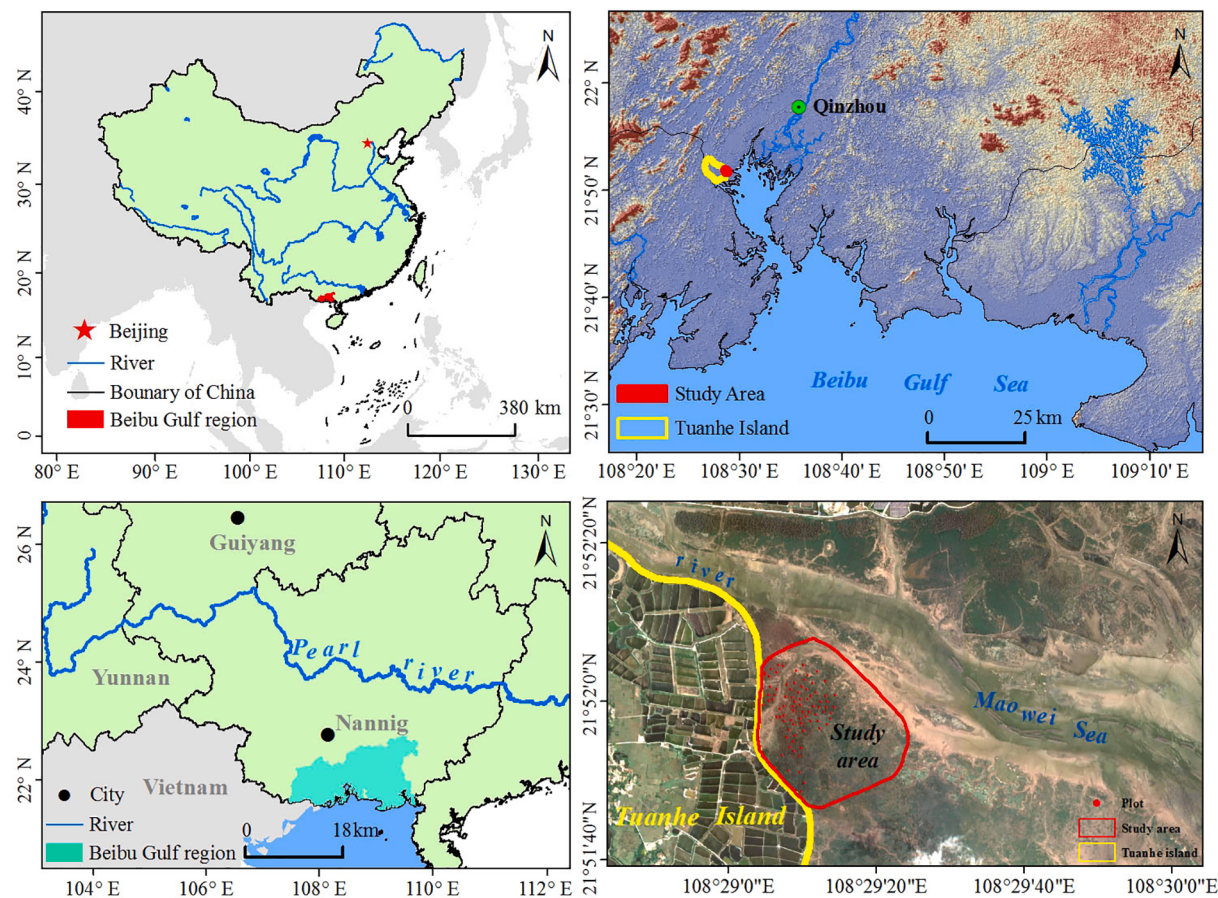


Fig. 1. Location map of research area (a,b,c) and plot field(d).

students to conduct a sample plot survey of *Sonneratia apetala* in the bund area of Tuanhe Island. A total of 84 quadrats were selected to conduct a survey of mangrove trees, and the single tree height and DBH parameters of each *Sonneratia apetala* were measured (1.3 m was the measured height of *Sonneratia apetala* DBH). The quadrats were 10 × 10 m in size. The coverage, soil PH, and soil salinity of the sample plots were also measured. The data of 84 mangrove quadrats obtained from the survey were used for modelling, of which 80% of the sample areas (67) were used for model training, and 20% of the sample areas (17) were used for model testing.

2.2.2. Calculation of aboveground biomass of sample plot by allometric growth equation

Mangrove is a special forest type that grows on beaches periodically submerged in seawater. The forest grows rapidly, given that *Sonneratia apetala* is a fast-growing and high-yield tree species. Tree species have been widely propagated in the bund area of Tuanhe Island since their introduction into the Kangxiling area, and most of them have grown into dense forests. The calculation of biomass by cutting standard trees causes a certain degree of damage to forested tree species. Therefore, this study estimates the AGB of *Sonneratia apetala* in the Tuanhe Island bund area using an allometric growth equation (Hu et al., 2019). The tree height parameters and DBH parameters (DBH at the measured height of 1.3 m) of *Sonneratia apetala* were mainly considered in the calculation. The specific calculation methods are presented in Table 1.

2.2.3. UAV aerial photography and laser point cloud data generation

In this study, a bumblebee four-rotor UAV was used to conduct aerial photography of the mangrove laser point cloud in the study area. Bumblebee UAV equipment was equipped with an AS-900HL multi-platform LiDAR scanning system (Fig. 3). Table 2 lists the detailed

parameters of the UAV-LiDAR system. The multiple echo technology of AS-900HL LiDAR can penetrate vegetation, quickly obtain high-precision laser point clouds under complex terrain conditions, and obtain complex three-dimensional mangrove laser point cloud data.

(1) Bumblebee UAV data acquisition

Before UAV flight, it needs to go to the field first. The field survey mainly checks whether high-voltage towers, communication towers, tall buildings, and other factors affect UAV flight safety in the study area. Given that the operation area of the project is in the bund area of Tuanhe Island, the terrain is flat, and no high-pressure towers and tall buildings, which will affect aircraft flight, are present. On January 20, 2021 the project selected cloudless, sunny weather, and low tide levels to collect data from the *Sonneratia apetala* laser point cloud. The aircraft took off at the open seawall in the Maowei Sea (Fig. 3(b)). After the site survey, a suitable location was selected to erect the base station according to the site survey conditions. The base station erection was controlled within a radius of 5 km to ensure that the satellite observation altitude angle was within 15°, the number of observation satellites was not less than 18, and the base station sampling rate was set to 5 Hz (Fig. 3(c)). After the base station is laid, the route should be set according to the actual situation of the study area and the requirements of measurement accuracy. The navigation height of the test area selected for this operation was 70 m, the distance of the route was 30 m, the flight speed was 6 m/s, the lateral overlap rate was 70%, and the course overlap rate was 80%. Fig. 3(d) shows the parameter setting process before the UAV flight. After the flight parameters were set, data were collected using hand-held software, and the laser line speed in the test area was set at 120 lines/s. After checking that the UAV and LiDAR settings were correct, the UAV-LiDAR was left standing for nearly 3 min before take-off to ensure the accuracy requirements. In the meantime, to avoid the error accumulation of the inertial measurement unit (IMU), the UAV flies in the

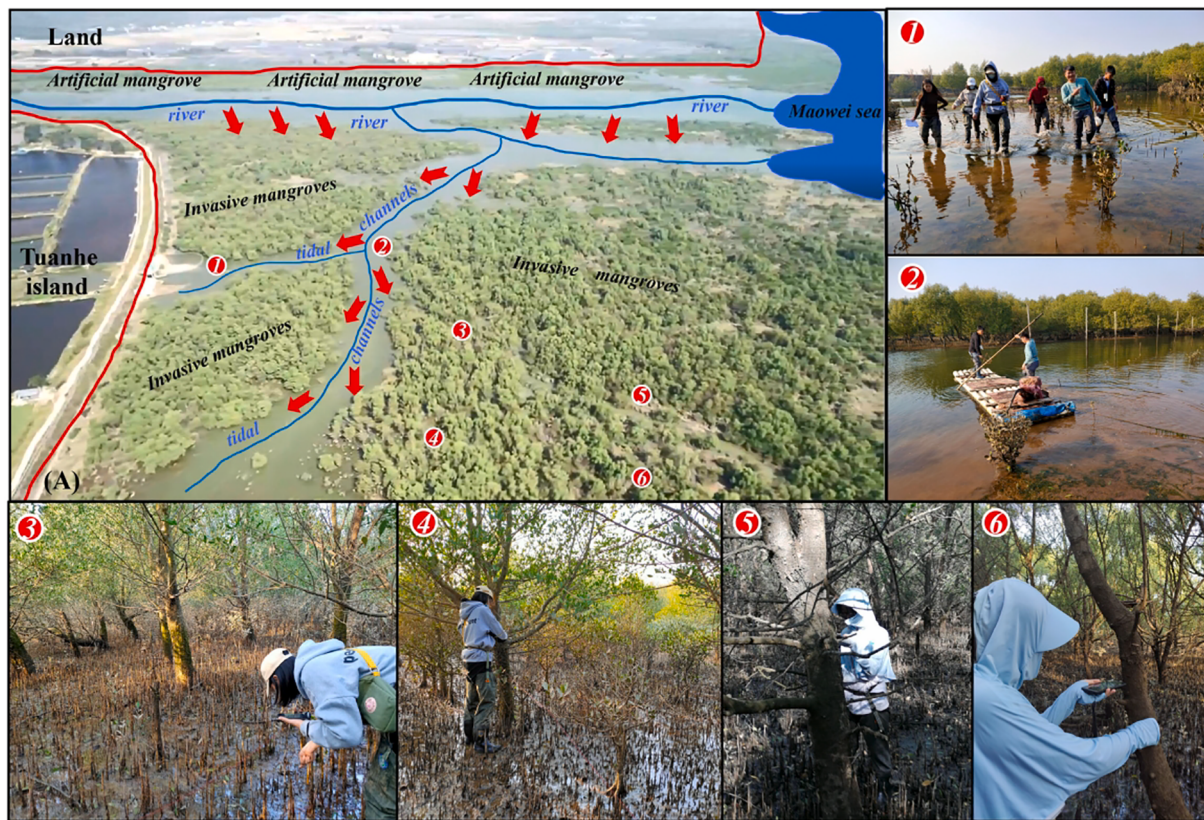


Fig. 2. Invasive mangrove diffusion process (A), *Sonneratia apetala* community (①②), Mangrove tidal channels crossing process (③), Measurement of 1.3 m-diameter *Sonneratia apetala* (④⑤⑥).

Table 1
Allometric growth equations of mangrove in study area.

| Plant species | Plant species | Allometric growth equation | References |
|---------------------------|---------------|---|-------------------|
| <i>Sonneratia apetala</i> | Stem | $B_{\text{stem}} = 0.022 \times (DBH^2 \times H)^{0.937}$ | (Hu et al., 2019) |
| | Branch | $B_{\text{branch}} = 0.011 \times (DBH^2 \times H)^{0.957}$ | |
| | Leaf | $B_{\text{leaf}} = 0.002 \times (DBH^2 \times H)^{0.905}$ | |
| | AGB | $B_{\text{AGB}} = 0.034 \times (DBH^2 \times H)^{0.966}$ | |

CD:Canopy diameter(cm); DBH: diameter at breast height (m); H: height (m); B_{AGB} : aboveground biomass (kg); B_{stem} : stem biomass (kg); B_{branch} : branch biomass (kg); B_{leaf} : leaf biomass (g).

shape of ‘8’ after entering the sky over the survey area, and then data acquisition is conducted according to the route planning. Fig. 3(e) shows the takeoff process of the UAV. After the data acquisition in the test area was completed, the surrounding environment was observed before landing to ensure landing safety. After landing, the UAV-LiDAR stood for approximately 3 min.

(2) Laser point cloud data processing

After data acquisition, the data need to be processed in the office. Office data processing is mainly divided into a position and orientation system (POS) position solution and point cloud solution. During the POS position calculation, the base station and POS data (mainly including mobile station GPS and IMU data) need to be combined to output high-precision positioning and attitude data. Then, internal explorer post-processing software is used to process the GNSS data to obtain high-precision combined navigation information such as position, speed, and attitude. The UAV-LiDAR system records the measurement data for

each sensor. These data must be registered and fused according to the measurement model (timing and position parameters of each sensor) to restore the three-dimensional geometric space coordinates and attributes of the measured target. This method is called a point-cloud solution. Fig. 4 shows the calculated three-dimensional laser point cloud information of *Sonneratia apetala*. Fig. 4(a) shows the laser point cloud data of the study area, Fig. 4(b) is the profile, and Fig. 4(c) shows the enlarged detail of the laser point cloud. Through field investigation and combined with laser point cloud information, ① in Fig. 4(c) is the point cloud information of the *Sonneratia apetala* community, ② is the beach ground point cloud information, and ③ is the point cloud information absorbed by water due to the influence of tidal ditch water. Therefore, no laser point cloud echo information is available. The coordinates of the laser point cloud collected by the UAV-LiDAR system in the experimental area of *Sonneratia apetala* are all longitude, latitude, and ellipsoid height under the WGS84 ellipsoid, and the corresponding projection coordinates are CGCS2000 projection coordinates.

(3) Laser point cloud data processing and variable generation

Laser point cloud data in the las1.4 standard format can be obtained after the point cloud solution. The echo information of each point cloud includes a three-dimensional coordinate value (x, y, z), intensity value, and return type (Tian et al., 2021). The data processing of the *Sonneratia apetala* laser point cloud mainly includes the segmentation of ground point clouds and non-ground point clouds. The segmentation algorithm adopted a combined filter cloth algorithm (Li, 2020). After segmentation, the *Sonneratia apetala* laser point cloud above the ground can be obtained, which can generate the intensity and height variables used in this study (Table 3). For the extraction of these variables, the mangrove aboveground biomass retrieval system based UAV-LiDAR (LiMARS system hereinafter) independently developed by our team was selected for this study. The system is mainly composed of a laser point cloud data processing module and a biomass retrieval module. The laser point cloud



Fig. 3. UAV-LiDAR system composition (a), UAV takeoff position(b), RTK positioning equipment (c),Commissioning of UAV equipment and laser point cloud carrying process (d), and Initial stage of UAV takeoff (e).

Table 2
Composition and parameters of UAV-LiDAR system.

| Composition | Content | Parameter |
|------------------------------------|-----------------------------------|--|
| System architecture | weight | 4.7kg |
| | absolute precision | horizon 5cm,vertical 5cm |
| | operating | -10°C to +40°C |
| | temperature range | |
| | supply voltage | 24V |
| | power consumption | 65W |
| | Laser level | Level 1 |
| | line number | unifilar |
| | maximum detection range | 920 m |
| | minimum detectable range | 3 m |
| Laser scanning system | survey precision | 10mm, repeatability precision 5mm |
| | field of view | 330° |
| | scanning frequency | 10~200Hz |
| | weight | 3.75kg |
| | Laser emission frequency | 550,000 HP/SEC |
| | effective pixels | 2430 myriad |
| | resolution | 6000×4000 |
| | Car panoramic photo pixels | 30MP |
| Camera system (upgradeable) | Data update frequency | 200Hz |
| | zero bias stability | 0.05°/h |
| | Angle input range | ±490°/s |
| | Accelerometer range | ±10g |
| | Zero deviation of accelerometer | 7.5mg |
| | Postprocessing attitude accuracy | Roll/Pitch: 0.005° Heading: 0.017° |
| | Post processing position accuracy | horizon:0.01m elevation:0.02m |
| Positioning and orientation system | GNSS | Can receive three bands L-band, SBAS, QZSS GPS, GLONASS, Beidou ephemeris data, support single antenna and dual antenna work |

data processing module mainly includes ground point cloud and non-ground point cloud segmentation, digital elevation model extraction, digital surface model extraction, canopy height model extraction, single tree segmentation, height variable extraction, intensity variable extraction, and canopy density. Meanwhile, the biomass inversion module mainly includes extreme learning machine learning algorithms, support vector regression (SVR) algorithms, Random forest regression (RFR) algorithms, boosting algorithms, and neural network algorithms. The specific modules are shown in Fig. 5. UAV laser remote sensing data can derive a large number of height and intensity variables. Thus, on the basis of the LiMARS system developed by our team, this study extracts the height variables (35) and intensity variables (26) of the laser point cloud to conduct mangrove biomass inversion based on the non-ground point cloud data of *Sonneratia apetala*. The point cloud characteristic parameter variables and their specific descriptions are listed in Table 3.

2.3. Methods

2.3.1. Technical process

Based on the UAV-LiDAR point cloud data and the measured mangrove aboveground sample survey data, four machine learning methods were used to invert the AGB of invasive mangroves in the Tuanhe Island bund area. According to the inversion results, the effects of different hydrological response units, beach height, and main tidal channel on mangrove biomass were analysed. The detailed technical process is shown in Fig. 6. The first step is data acquisition and processing, including UAV data processing and field data investigation. The first part is UAV laser point cloud data processing, including bumblebee aerial photography, base station erection, and laser point cloud data calculation. The second part is the investigation of mangrove tree species in *Sonneratia apetala*, which mainly involves the investigation of mangrove tree height, DBH, and other parameters. The second step was feature extraction. According to the normalised laser point cloud, this study generates the height feature variables of the laser point cloud (35 in total), the intensity feature variables of the laser point cloud (26 in

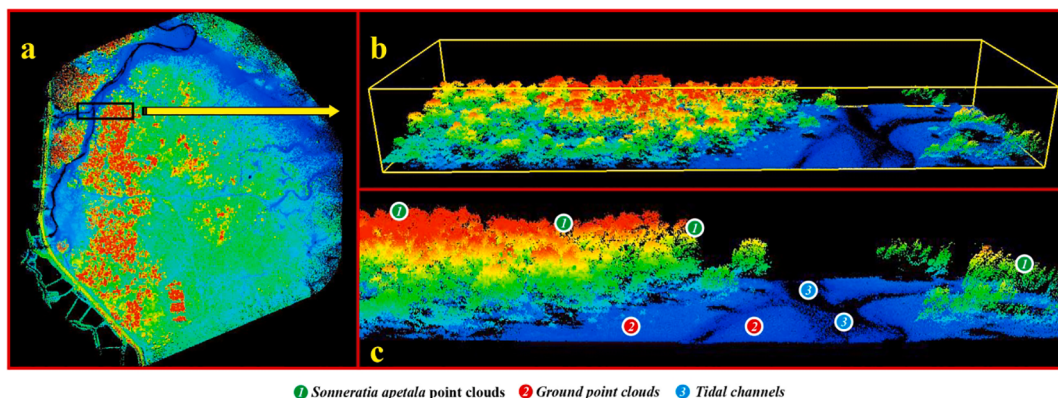


Fig. 4. Laser point cloud acquired by UAV (a), local magnification of laser point cloud profile (b), and three different laser point cloud details display information, namely, *Sonneratia apetala* point clouds, Ground point clouds and Tidal channels point clouds (c).

total), and the combination of height and intensity feature variables (61 in total), and 38 variables selected by variable importance. In the third step, the measured mangrove sample plot data set was randomly divided, in which 80% (67) of the samples were used to train the model and 20% (17) of the samples were used to test the model. The initial parameters of the model are set according to the characteristics of the four machine learning algorithms, and then, the parameter parameters and parameter range are set according to different machine learning algorithms. The 10-fold crossover method was used to select the parameters, and all machine models were evaluated by R^2 and RMSE to screen the best machine learning model. In the fourth step, the optimal machine learning algorithm was used to map the mangrove AGB in the study area. In the fifth step, the quantitative relationship between the AGB of *Sonneratia apetala* and the beach landform and hydrological response unit was analysed.

2.3.2. Machine learning algorithm

In this study, four different machine learning algorithms, namely, XGBR, CBR, LGBR, and ABR, were selected to estimate the biomass of invasive mangroves. The specific principles of the different machine-learning algorithms are as follows:

(1) XGBR

Extreme gradient lifting (xgboost) is a new gradient-enhanced machine learning algorithm proposed by Chen and Guestrin in 2016 (Chen and Guestrin, 2016). The Xgboost model aims to prevent over-fitting and reduce the computational cost by maintaining the best computational efficiency of prediction through simplification and regularisation. The Xgboost algorithm originates from the concept of ‘promotion’. It combines all the predictions of a group of weak learners and trains strong learners through special training.

(2) GBR

The GBR gradient lifting decision tree (catboost) is a new gradient lifting decision tree (gbdt) algorithm. It successfully processes the classification features and uses classification features in the training process instead of preprocessing. Another advantage of the algorithm is that it uses a new pattern to calculate the leaf value when selecting the tree structure, which helps reduce overfitting and allows the use of the entire training dataset. Specifically, it randomly arranges each example dataset and calculates the average value of the example. For the regression task, the average value of the obtained data must be used for a priori calculation (Friedman, 2001; Dorogush et al., 2018).

(3) LGBR

Lightgbr is an open source, fast, and efficient promotion framework based on the decision tree algorithm, which supports efficient parallel training. The model was first proposed by the Microsoft team in 2017 and is an improved gradient lifting decision tree framework. Its basic idea is to linearly combine m weak regression trees into strong regression trees. The main improvements of the model include a histogram

algorithm and a leaf-wise strategy with depth constraints (Zhou et al., 2019a; Zhou et al., 2019b). The histogram algorithm divides the continuous data into k integers and constructs a histogram with width K. During traversal, the discretised value is accumulated in the histogram as an index, and then, the optimal decision tree segmentation point is searched. The leaf-wise strategy with depth limit refers to finding the leaf with the maximum gain to split and cycle each time. At the same time, the complexity of the model is reduced and overfitting is prevented by limiting the depth of the tree and the number of leaves.

(4) ABR

The principle of the AdaBoost algorithm combines the outputs of many ‘weak’ classifiers to produce effective classification. Its main process is to input samples and a weak learning algorithm first, randomly select n groups of data from the samples for training the model and assign 1/N weight to each group of data. Then, the weak learning algorithm is used to iterate the data t times. After each operation, the data weight was reassigned according to the classification results. In the next iterative calculation, the data that fail to be classified are given greater weight and receive more attention. Each weak classifier obtains a classification function, and these functions are assigned weight values. The corresponding weight value was greater when the classification results were better. After t iterations, the weighted results of all weak classification functions are strong classification functions (Dong et al., 2013).

2.3.3. Model evaluation

(1) Model optimal parameter setting

In this study, 84 mangrove quadrat data obtained through investigation were used for machine learning modelling, of which 80% of the sample areas (67) were used for model training, and 20% of the sample areas (17) were used for model testing and verification. When constructing different machine learning model parameters, the initial values are first set according to the characteristics of the different models. Then, the grid search method was used to optimise the super parameters (Lin et al., 2015). After hyperparameter optimisation, the best parameters of the different machine learning algorithms were obtained. Different machine learning models were constructed based on the best parameters. The best parameters of the four machine learning models are listed in Table 4.

(2) Importance of variables

When selecting four machine learning algorithm models, we input all laser point cloud height and intensity features (a total of 61 features) into different machine learning models, and 10 CV searches were conducted for hyperparametric adjustment (Table 4).

The best model was selected according to the root mean square error (RMSE) and the maximum R^2 value calculated by different models, and the judgment criteria were the minimum RMSE and maximum R^2 value. The highest prediction models of different feature combination

Table 3

Variables of above ground biomass inversion model of mangrove and their implications.

| Parameter type | Parameter number | Parameter Name | Explanation | References |
|--|------------------|---|---|---------------------|
| Height statistics of Lidar point cloud (HSLPC) | 1 | 1st_cover_above_mean (1st_cvme) | ((# of first returns > mean height of all returns) / (total # of first returns in the pixel)) * 100 | (Wang et al., 2020) |
| | 2 | 1st_cover_above_mode (1st_cvmo) | ((# of first returns > mode height of all returns) / (total # of first returns in the pixel)) * 100 | |
| | 3 | 1st_cover_above0.5 (1st_ca) | ((# of first returns >0.5 m) / (total # of first returns in the pixel)) * 100 | |
| | 4 | all_1st_cover_above_mean (all_1st_came) | ((# of all returns > mean height) / (total # of first returns in the pixel)) * 100 | |
| | 5 | all_1st_cover_above_mode (all_1st_camo) | ((# of all returns > mode height) / (total # of first returns in the pixel)) * 100 | |
| | 6 | all_1st_cover_above0.5 (all_1st_ca) | ((# of all returns >0.5 m) / (total # of first returns in the pixel)) * 100 | |
| | 7 | all_cover_above_mean (all_cvme) | ((# of all returns > mean height) / (total # of all returns in the pixel)) * 100 | |
| | 8 | all_cover_above_mode (all_cvmo) | ((# of all returns > mode height) / (total # of all returns in the pixel)) * 100 | |
| | 9 | all_cover_above0.5(all_ca) | ((# of all returns >0.5 m) / (total # of all returns in the pixel)) * 100 | |
| 10 | H_P01 | Height 1th percentile | (Wang et al., 2020) | |
| 11 | H_P05 | Height 5th percentile | | |
| 12 | H_P10 | Height 10th percentile | | |
| 13 | H_P20 | Height 20th percentile | | |
| 14 | H_P25 | Height 25th percentile | | |
| 15 | H_P30 | Height 30th percentile | | |
| 16 | H_P40 | Height 40th percentile | | |
| 17 | H_P50 | Height 50th percentile | | |

Table 3 (continued)

| Parameter type | Parameter number | Parameter Name | Explanation | References |
|---|------------------|----------------|--|------------|
| | 18 | H_P60 | Height 60th percentile | |
| | 19 | H_P70 | Height 70th percentile | |
| | 20 | H_P75 | Height 75th percentile | |
| | 21 | H_P80 | Height 80th percentile | |
| | 22 | H_P90 | Height 90th percentile | |
| | 23 | H_P95 | Height 95th percentile | |
| | 24 | H_P99 | Height 99th percentile | |
| | 25 | H_AAD | Average absolute deviation of point cloud height | |
| | 26 | H_Cv | Coefficient of variation of point cloud height | |
| | 27 | H_IQ | Height 75th percentile minus 25th percentile | |
| | 28 | H_Kurtosis | Kurtosis of point cloud height | |
| | 29 | H_Skewness | Skewness of point cloud height | |
| | 30 | H_stddev | Standard deviation of point cloud height | |
| | 31 | H_variance | Variance of point cloud height | |
| | 32 | H_mean | Average of point cloud height | |
| | 33 | H_max | Maximum of point cloud height | |
| | 34 | H_min | Minimum of point cloud height | |
| | 35 | H_mode | Mode of point cloud height | |
| Intensity statistics of Lidar point cloud (LSLPC) | 1 | I_P01 | Intensity 1th percentile | |
| | 2 | I_P05 | Intensity 5th percentile | |
| | 3 | I_P10 | Intensity 10th percentile | |
| | 4 | I_P20 | Intensity 20th percentile | |
| | 5 | I_P25 | Intensity 25th percentile | |
| | 6 | I_P30 | Intensity 30th percentile | |
| | 7 | I_P40 | Intensity 40th percentile | |
| | 8 | I_P50 | Intensity 50th percentile | |
| | 9 | I_P60 | Intensity 60th percentile | |
| | 10 | I_P70 | Intensity 70th percentile | |
| | 11 | I_P75 | Intensity 75th percentile | |
| | 12 | I_P80 | Intensity 80th percentile | |

(continued on next page)

Table 3 (continued)

| Parameter type | Parameter number | Parameter Name | Explanation | References |
|----------------|------------------|----------------|---|--|
| | 13 | I_P90 | Intensity 90th percentile | |
| | 14 | I_P95 | Intensity 95th percentile | |
| | 15 | I_P99 | Intensity 99th percentile | |
| | 16 | I_AAD | Average absolute deviation of point cloud intensity | (Wang et al., 2020; Yuan et al., 2021) |
| | 17 | I_Cv | Coefficient of variation of point cloud intensity | |
| | 18 | I_IQ | Intensity 75th percentile minus 25th percentile | |
| | 19 | I_Kurtosis | Kurtosis of point cloud intensity | |
| | 20 | I_Skewness | Skewness of point cloud intensity | |
| | 21 | I_stddev | Standard deviation of point cloud intensity | |
| | 22 | I_variance | Variance of point cloud intensity | |
| | 23 | I_mean | Average of point cloud intensity | |
| | 24 | I_max | Maximum of point cloud intensity | |
| | 25 | I_min | Minimum of point cloud intensity | |
| | 26 | I_mode | Mode of point cloud intensity | |

scenarios of LHI, LII, and AI were tested on the basis of the selected best model. This study also used RMSE and R^2 to determine the advantages and disadvantages of the model. Finally, the mangrove biomass was retrieved according to the selected optimal characteristic parameters. To screen the importance of feature variables, the feature selector tool developed by Koehrsen (2019) was used for feature selection, and the algorithm was implemented in Python 3.6.

(3) Evaluation of the model accuracy

This study selected two common indicators for model verification, namely, R^2 and RMSE, to verify the precision relationship between mangrove biomass predicted by the machine learning model and field survey biomass (Lu et al., 2014). The RMSE value is closer to 0 when R^2 is closer to 1, which means that the predicted biomass accuracy of the model is higher (Tian et al., 2021).

The calculation formula of each variable is as follows:

$$R^2 = 1 - \frac{\sum_{i=1}^n (y_i - \hat{y}_i)^2}{\sum_{i=1}^n (y_i - \bar{y}_i)^2} \quad (1)$$

$$RMSE = \sqrt{\frac{\sum_{i=1}^n (y_i - \hat{y}_i)^2}{n}} \quad (2)$$

In the above formula, y_i is the biomass of the measured sample plot. \bar{y}_i is the average value of the measured mangrove. \hat{y}_i is the predicted

mangrove biomass and i is the amount of data in the equation.

2.3.4. Hydrological response unit extraction

In recent years, the tools for extracting watershed features are mainly ArcGIS 10.5 and ArcHydro software, the soil and water assessment tool (SWAT) and ArcHydro tools (Arnold et al., 1998; Sadeghi et al., 2021). ArcHydro tools is directly built into ArcGIS10.5 software and is a popular hydrological data model for extracting hydrological characteristics of river. Therefore, this paper mainly uses ArcHydro tools in ArcGIS10.5 to extract tidal ditches and generate subbasins in the study area (Sadeghi et al., 2021). It mainly includes six steps: filling depression with DEM data, determining the direction of water flow, determining the accumulation of confluence, setting the threshold of catchment area, generating subbasins and tidal gully system (Sadeghi et al., 2021).

3. Results and analysis

3.1. Growth of *Sonneratia apetala*

Table 5 shows the data of tree height, DBH, and density in the field investigation of *Sonneratia apetala*. Field investigations show that the average tree height of *Sonneratia apetala* is 8.23 m, which is lower than that of the artificial *Sonneratia apetala* in the north (11.82 m) (Tian et al., 2021). The average DBH at 1.3 m was 15.52 cm, which is also lower than the calculated DBH of artificially planted *Sonneratia apetala* in the Beibu Gulf area (20.73 cm). The trees in the community are densely distributed, with 865 trees per square hectare, most of which were diffused *Sonneratia apetala* seedlings. The AGB value calculated by *Sonneratia apetala* allometric growth equation is 5.46–135.60 Mg/ha, and the average value is 27.32 Mg/ha, which is lower than the aboveground biomass of *Sonneratia apetala* in the north (Tian et al., 2021).

3.2. Modelling results, assessment and comparison

Figs. 7 and 8 and **Table 6** compare the effects of the four machine learning algorithms on mangrove biomass fitting. The input variables of the four models are 61, including 35 height characteristic variables and 26 intensity characteristic variables generated by the laser point cloud. According to the calculation results, CBR shows a good fitting effect in the four machine learning models, and its R^2 exceeds 0.7190 in the testing and training phases. The RMSE is the smallest among the four models, and its value is 13.8728 Mg/ha. The simulation effect of the representative model fits well with the field investigation effect. The model with a good fitting effect is the ABR model, which has a high R^2 of 0.6544 and RMSE of 15.3851 Mg/ha in the testing phase. In contrast, the fitting effect of the LGBR machine regression model in this study is poor, and the ability to simulate and predict biomass in the study area is poor. Therefore, it is unsuitable for simulating mangrove biomass.

The CBR model showed good results for mangrove biomass fitting. This study uses the CBR machine learning model to test the fitting effect of four different variable combination scenarios: LHI, LII, of and AI. **Table 7** shows that the fitting effect of the combined model with 35 height characteristic variables and 26 strength characteristic variables under the support of the same machine learning model CBR is poor, with R^2 values of 0.4725 and 0.5127, respectively, which do not exceed 0.60. This result shows that, when fitting the mangrove biomass model of *Sonneratia apetala*, using only height and intensity variables cannot make the predicted results close to the measured real value. However, the feature selector tool developed by WillKoehrsen (2019) was used for feature engineering selection for all variables, and 38 variables were considered in the CBR model. The model shows a high fitting ability. R^2 reaches 0.7644 and RMSE is 11.1725 Mg/ha in the testing phase, which are relatively better than the fitting results using all characteristic variables (61 predictive variables). R^2 increases by 0.0454 and the RMSE decreases by 2.7003 Mg/ha in the testing phase. The results show that 38 variables selected by characteristic variables can be used to predict

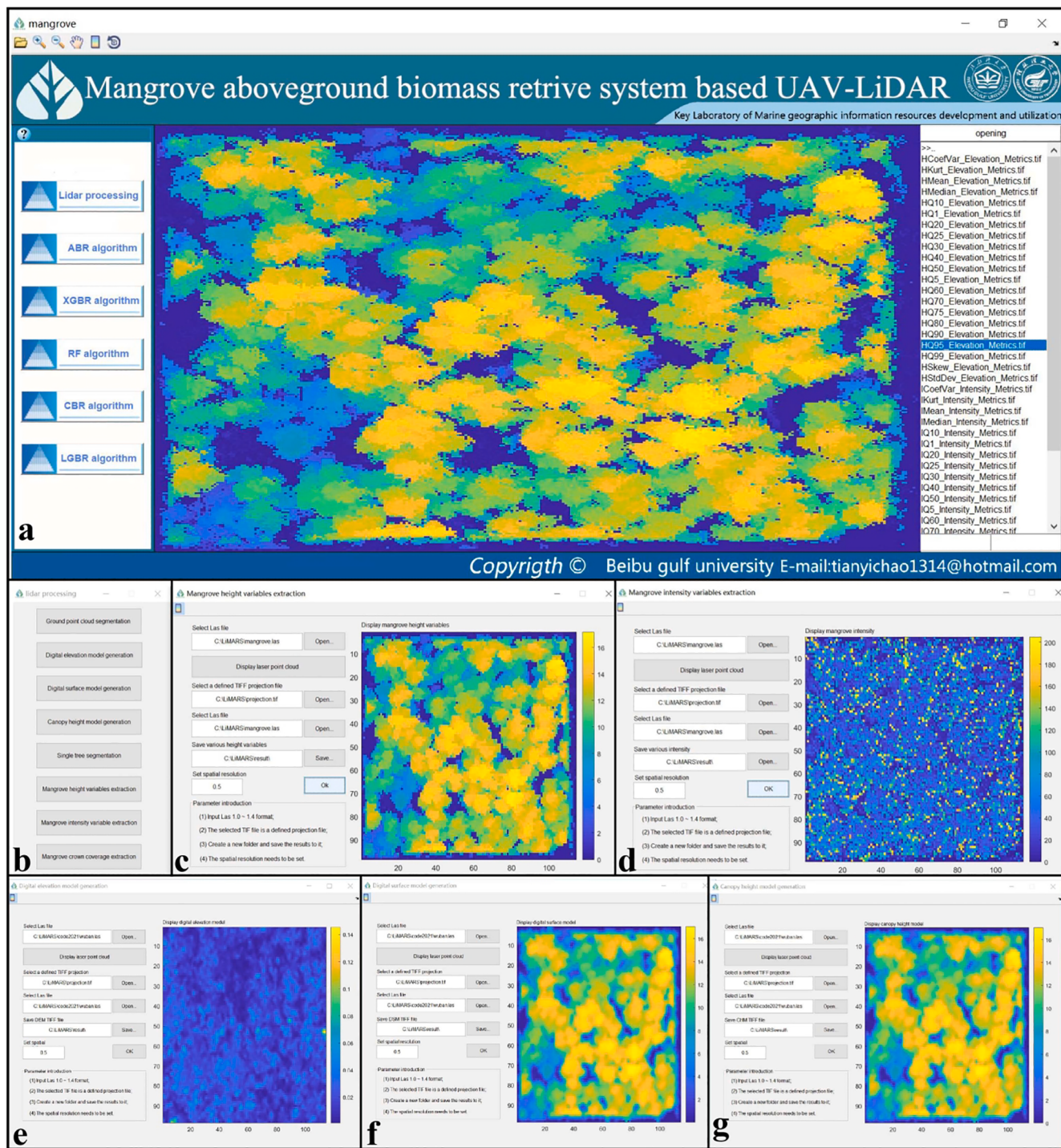


Fig. 5. Mangroove aboveground biomass retrive system based UAV-LiDAR (LiMARS system)(a), Lidar processing toolboxes(b), Mangrove height variables extraction modules(c), Mangrove intensity variables extraction modules(d), Digital elevation model generation modules(e), Digital surface model generation generation modules(f) and Canopy height model generation modules(g).

mangrove biomass in the study area.

We used 38 optimal characteristic variables to test the accuracy of four machine learning models, namely, XGBR, CBR, LGBR, and ABR, to verify whether the CBR model is the optimal model for estimating the *Sonneratia apetala* in the study area (Table 8). The CBR obtained excellent results according to the test results. In the testing phase, R^2 is 0.7644 and the RMSE is 11.1725 Mg/ha. The second is the XGBR and ABR models, with RMSE of 13.1052 and 13.6533 Mg/ha, respectively. Meanwhile, the fitting effect of the LGBR model is poor, with an RMSE of 18.5510 Mg/ha. The abovementioned analysis results show that CBR

can predict the aboveground biomass of invasive *Sonneratia apetala*.

3.3. Variable importance

In this study, all 37 variables were placed into the feature selector tool to identify the importance of 61 characteristic variables for mangrove AGB. The degree of importance is represented by the normalised importance. Fig. 9 shows the selection results of the variable importance, and Fig. 10 shows the results of the cumulative variable importance. According to the variable selection results, the parameters

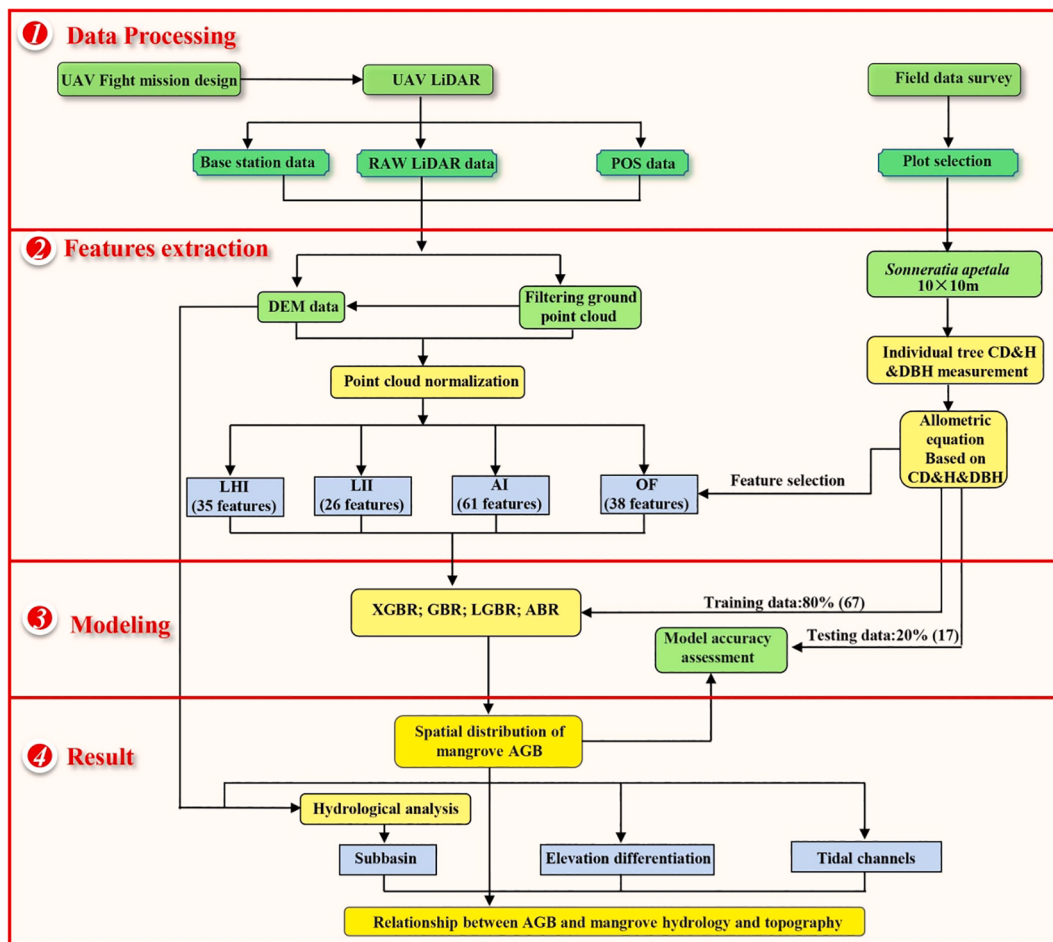


Fig. 6. Flowchart for UAV data processing, laser point cloud variable extraction, modeling process and result analysis in study area.

Table 4
Hyperparameters of different machine learning models in this study.

| Machine Learning Model | learning rate epsilon | Min samples leaf weight | Min child weight | Gamma random_state | Max depth Max features | n_estimators n_neighbors |
|---|--------------------------|----------------------------|---------------------|-----------------------|------------------------------|-----------------------------|
| XGBoost Regressor(XGBR) | 0.10 | 4 | | 0.10 | 3 | 230 |
| CatBoost Regressor(CBR) | 0.05 | NA | | NA | 6 | 100 |
| Light Gradient Boosting Regressor (LGBR) | 0.05 | 1 | | NA | 5 | 100 |
| AdaBoost Regressor(ABR) | 0.01 | 30 | | 0 | NA | 60 |

Table 5
Mangrove growth statistics based on field sample-plot survey.

| Plant species | Plant height(H, m) | | Diameter at breast height(DBH, cm) | | AGB(Mg/ha) | | Standard deviation (Mg/ha) SD | Tree density (tree/ha) Average |
|---------------------------|--------------------|--------------|------------------------------------|-------------|------------|---------------|----------------------------------|-----------------------------------|
| | Average | Range | Average | Range | Average | Range | | |
| <i>Sonneratia apetala</i> | 8.23 ± 1.23b | 1.55 ~ 13.58 | 15.52 ± 1.65a | 0.7 ~ 41.01 | 25.57 | 7.31 ~ 114.03 | 32.85 | 865 |

The data in the table are expressed as mean ± standard error; a indicate a significant difference (p less than 0.05) after the Tukey's honestly significant difference test amongst the different tree species through one-way

in the top five are the most sensitive to the contribution of mangrove biomass, and the specific variables are I_P60, 1st_cvme, I_P10, H_IQ, and 1st_CV. Among these variables, height variables account for three, which are 1st_cvme, H_IQ, and 1st_cv. Among the variables that rank 6–10, three also contribute greatly to mangrove biomass, and the variables are all_cvme, H_StdDev, and H_Cv. Interestingly, the analysis results of the 10 variables show that the contribution of height variables to the model reaches 6, while the contribution of intensity

variables to the model is only 4. Therefore, the height variables of the laser point cloud show a good effect in the estimation of mangrove aboveground biomass, while the contribution of intensity variables is less. The analysis results of cumulative variable importance show that when the characteristic variables reach 38, the cumulative contribution rate of the model reaches more than 0.95, and the latter variables have a lower contribution rate to the model. Therefore, this study selected the first 38 variables to estimate the biomass of *Sonneratia apetala*. Among

Table 6

Precision comparison results of different machine learning methods using all features.

| NO | Machine Learning Model | R^2 Training (80%) | R^2 Testing (20%) | RMSE(Mg/ ha) |
|----|--|-------------------------|------------------------|-----------------|
| 1 | XGBoost Regressor(XGBR) | 0.9457 | 0.6402 | 15.6981 |
| 2 | CatBoost Regressor(CBR) | 0.8601* | 0.7190* | 13.8728* |
| 3 | Light Gradient Boosting Regressor(LGBR) | 0.6846 | 0.3687 | 20.7946 |
| 4 | AdaBoost Regressor(ABR) | 0.8775 | 0.6544 | 15.3851 |

*The best performance

the results of the first 38 variables, the contribution rate of the height variables is as high as 22, while the contribution rate of the intensity variables is only 16. This finding further confirms that height variables play an important role in the biomass inversion model. However, the analysis results in Table 7 indicate that some intensity variables need to be combined to improve the prediction accuracy of the model, considering that height variables alone cannot completely improve the prediction accuracy of the model.

3.4. Spatial distribution of mangrove biomass

Based on the selected 38 laser point cloud height variables and intensity, the CBR model was used to predict the biomass thematic map of invasive mangroves in the study area. Fig. 11 shows that the predicted value of mangrove biomass per unit area is between 7.31 and 114.04 Mg/ha, with an average value of 25.57 Mg/ha. From the perspective of spatial distribution, the biomass of *Sonneratia apetala* was higher in the western part of the study area, and its aboveground biomass was mainly more than 100 Mg/ha. The biomass of the *Sonneratia apetala* community in the east is relatively small, with a value of 20 Mg/ha. This is because *Sonneratia apetala* in the eastern part diffuses from the northern part along the tidal ditch. The age of *Sonneratia apetala* species is older than that in the eastern region, while most of the eastern region is young plants of *Sonneratia apetala*, with small biomass.

3.5. Relationship between mangrove AGB and geomorphic and hydrological response

Based on the ground point cloud information of the laser point cloud,

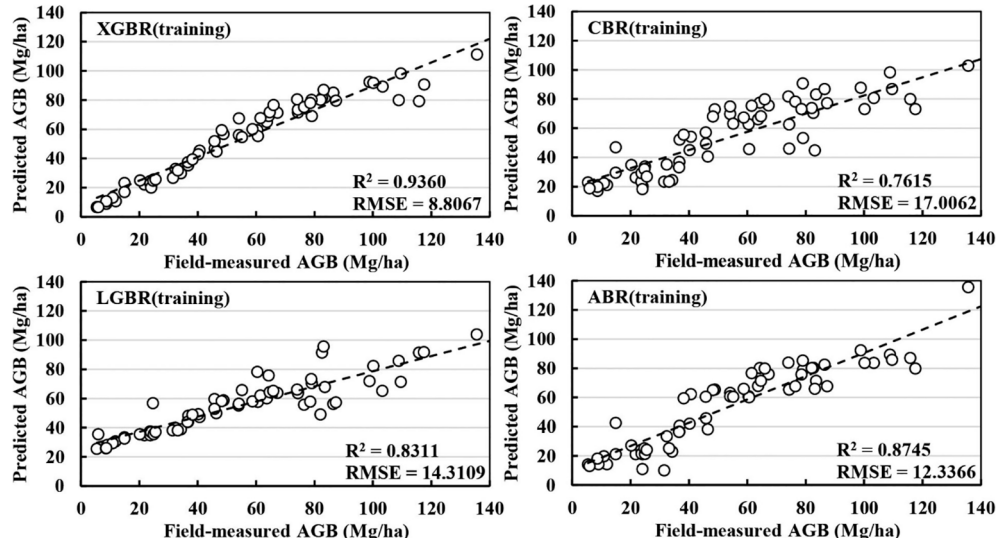


Fig. 7. Scatter plots of the field-measured (X axis) versus predicted (Y axis) mangrove AGB in the four different ML models(Training phase).

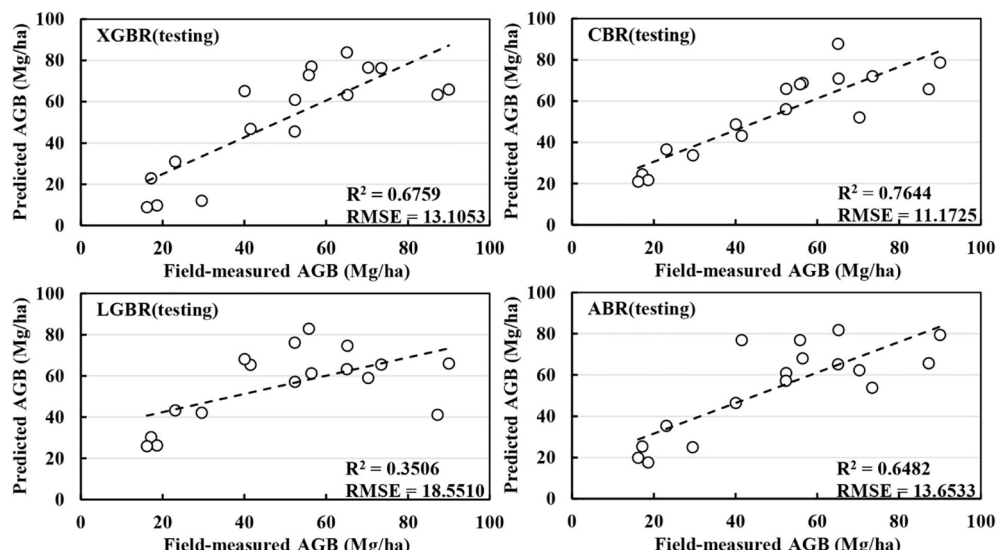


Fig. 8. Scatter plots of the field-measured (X axis) versus predicted (Y axis) mangrove AGB in the four different ML models(Testing phase).

Table 7
Performance of the CBR model using different numbers of variables.

| No | Input variables | R ² Training (80%) | R ² Testing (20%) | RMSE (Mg/ha) |
|-----|--|----------------------------------|---------------------------------|-----------------|
| LHI | 35 features form lidar height index(LHI) | 0.8822 | 0.4725 | 19.5245 |
| LII | 26 features from lidar indensity index(LII) | 0.8692 | 0.5127 | 18.7663 |
| OF | 38 optimal features(OF) from feature selection | 0.7615* | 0.7644* | 11.1725* |
| AI | 61 features form lidar height index and lidar indensity index (all indexs, AI) | 0.8601 | 0.7190 | 13.8728 |

Table 8
Precision comparison results of different machine learning methods using optimal features.

| NO | Machine Learning Model | R ² Training (80%) | R ² Testing (20%) | RMSE(Mg/ ha) |
|----|---|----------------------------------|---------------------------------|-----------------|
| 1 | XGBoost Regressor(XGBR) | 0.9360 | 0.6759 | 13.1053 |
| 2 | CatBoost Regressor(CBR) | 0.7615* | 0.7644* | 11.1725* |
| 3 | Light Gradient Boosting Regressor(LGBR) | 0.8311 | 0.3506 | 18.5510 |
| 4 | AdaBoost Regressor(ABR) | 0.8745 | 0.6482 | 13.6533 |

*The best performance.

the beach elevation spatial distribution map of the study area can be formed through inverse distance interpolation. The beach elevation was reclassified in this study and divided into six categories, as shown in Fig. 12, to more clearly reveal the impact of different beach elevations on mangrove biomass. We mapped the biomass differentiation of *Sonneratia apetala* at different elevations based on elevation classification data. Fig. 13 shows that the maximum biomass of *Sonneratia apetala* presents the maximum value in the second elevation zone of −0.97 m to

0.56 m, and the value of aboveground biomass is 28.97 Mg/ha. The AGB above or below this elevation shows a downward trend, which indicates that the interval of −0.97 m to 0.56 m is the best threshold interval for the survival of *Sonneratia apetala*.

This study extracts the hydrological response subbasin units in this area based on the tidal flat digital ground model and with the support of the ArcGIS hydrological analysis tool to reveal the impact of different hydrological response units and tidal ditch distance on AGB(Fig. 14(a)). At the same time, according to the GIS spatial analysis module, a spatial classification map of the distance from the tidal ditch is generated (Fig. 14(b)), and the AGB statistics of *Sonneratia apetala* in different hydrological units and the distance from the tidal ditch are shown in Fig. 15. Fig. 14(a) shows that the area of subbasin 1 is the largest, and its AGB also presents the maximum value, which is 32.68 Mg/ha. Although the area of subbasin 2 ranks second, the biomass of the subbasin has not shown the maximum value, but the minimum value of the region, which is only 19.07 Mg/ha. Therefore, the AGB of the invasive mangrove has nothing to do with the area of the hydrological response unit. From the spatial differentiation results of mangrove AGB far and near the tidal gully, the AGB of *Sonneratia apetala* showed the highest biomass within 100 m of the tidal gully, with a value of 41.89 Mg/ha. The AGB of *Sonneratia apetala* shows a downward trend with increasing distance, which implies that the size domain of *Sonneratia apetala* AGB is related to the distance from the main tidal gully. Specifically, the AGB was lower when the distance was greater.

4. Discussion

4.1. Selection of model characteristic parameters

With the development of multispectral remote sensing satellites, especially the addition of red edge bands and near-infrared bands, many scholars have used high-resolution satellite data such as SPOT4/5(Pham and Brabyn, 2017), GeoEye1(Jachowski et al., 2013), ALOS AVNIR2 (Wicaksono et al., 2016), WorldView2(Zhu et al., 2015), and Sentinel 2 (Castillo et al., 2017) of ESA to retrieve mangrove biomass. Most of these methods retrieve mangrove AGB based on each vegetation index. For example, Zhu et al. (2015) retrieved the AGB of mangrove forests with the help of a neural network based on field sample survey data and the relationship between vegetation spectral indexes of Worldview2. The Sentinel-2 satellite image has 13 bands, including 2 bands with a spatial resolution of 20 m, a red edge band for vegetation monitoring, and 4 traditional bands of red, green, blue, and near-infrared with spatial resolution of 10 m. Satellite data have many band data, which can build various rich and diverse vegetation indices that are suitable for mangrove biomass inversion. For example, Castillo et al. (2017) explored the inversion ability of different vegetation indices in the accuracy of mangrove biomass when Sentinel-2 and Sentinel-1 were combined. The results show that the vegetation index of Sentinel-2 alone can improve the estimation ability of the biomass model; however, excessive use of vegetation index to estimate biomass may cause some uncertainty in the inversion results, which is due to the over-fitting of the evaluation results of the model due to the possible over saturation of some vegetation indices such as NDVI(Yang et al., 2016; Song et al., 2006; Zhou et al., 2019a; Zhou et al., 2019b).

With the development of science and technology in recent years, LiDAR device has shown a trend of portability and miniaturisation, and the price is becoming increasingly cheaper, which provides convenience for the acquisition of laser point clouds (García et al., 2010). The laser point cloud method can extrapolate the structural and functional parameters of trees to a larger scale to obtain the structural parameters of trees in a larger region or the entire study area. For example, Huang et al. (2018) first combined the allometric growth model obtained from field sample survey data and the canopy height variable obtained from ICESat/GLAS data. Thus, the AGB in the ICESat/GLAS quadrat scale was determined. Then, they constructed an inversion model by using

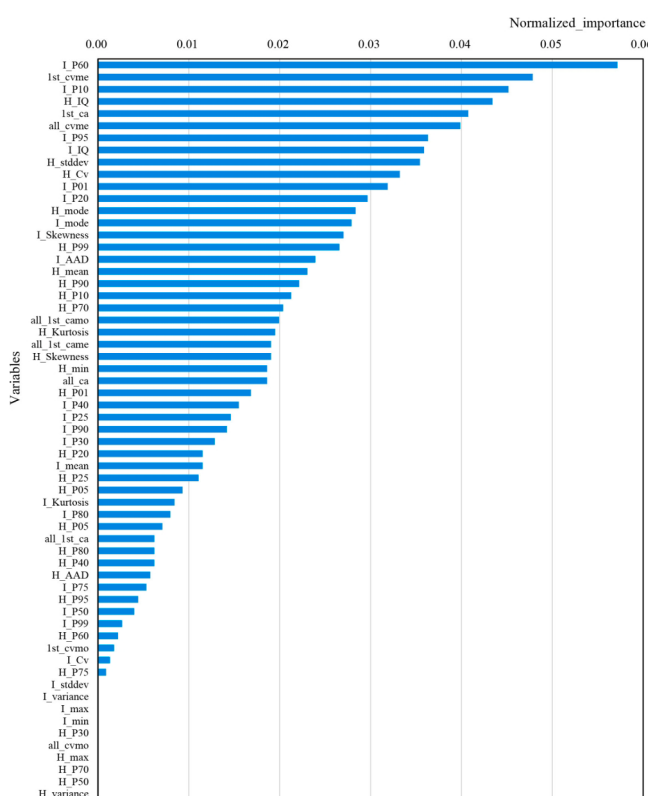


Fig. 9. Order of selected variable importance of mangroves in study area.

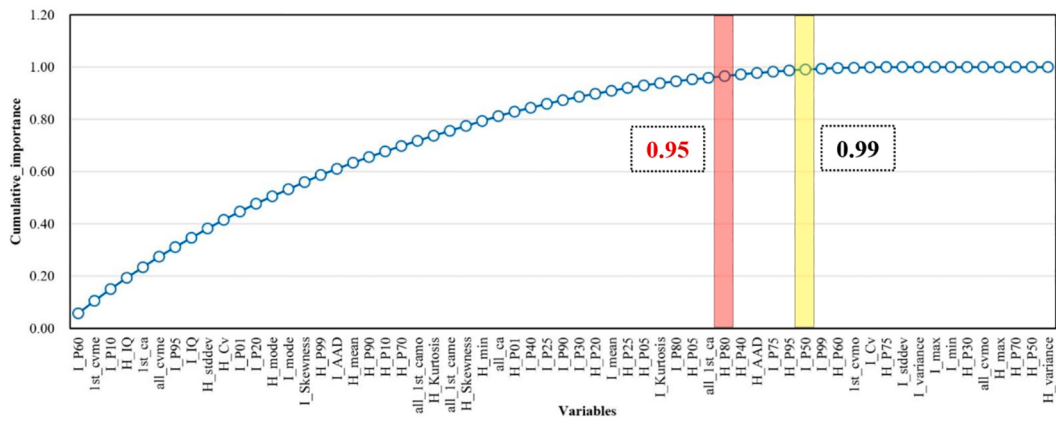


Fig. 10. Cumulative variable importance of mangroves in study area(The red color column represents the cumulative variable importance of 0.95, while the yellow color represents 0.99).

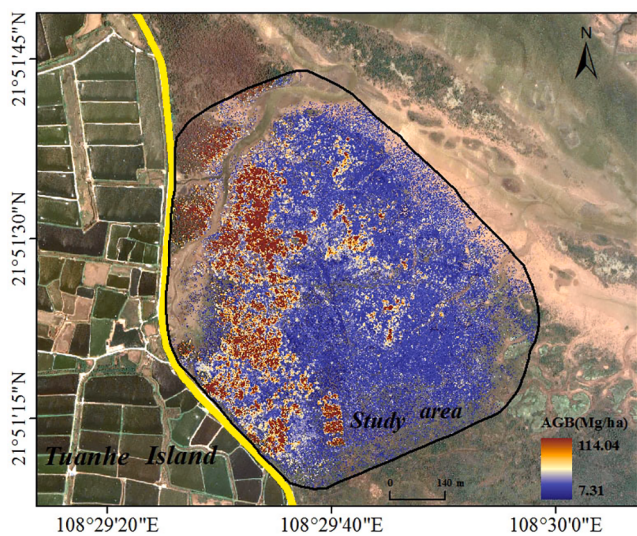


Fig. 11. Spatial distribution of aboveground biomass of mangroves retrieved by CBR methods.

medium-resolution satellite Landsat and PALSAR data and considering the AGB calculated in the ICESat/GLAS quadrat scale as training samples. They obtained a spatial distribution map of biomass with 30 m resolution in China scale. The idea of this study is consistent with that of Huang et al. (2018). This study estimates the AGB of *Sonneratia apetala*

on the basis of the survey results of AGB of *Sonneratia apetala*, with the support of the allometric growth equation, the measured AGB of the plot investigation as the training sample, and laser point cloud variables. The laser point cloud can obtain the three-dimensional structural parameter information of the trees. Thus, this three-dimensional information overcomes the defect of saturation of the vegetation index NDVI(Yang et al., 2016), and it is increasingly used to calculate the AGB of mangroves(Fatoyinbo et al., 2018; Feliciano et al., 2017; Hickey et al., 2018). For example, Fatoyinbo et al. (2018) constructed the AGB of mangroves based on field sample measurement data and LiDAR data in 2018. The calculation results show that the average tree height variable can significantly improve the accuracy of AGB estimation of mangroves.

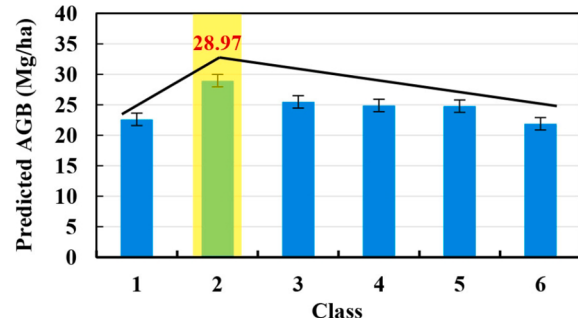


Fig. 13. Histogram of aboveground biomass of mangrove in different elevation ranges.

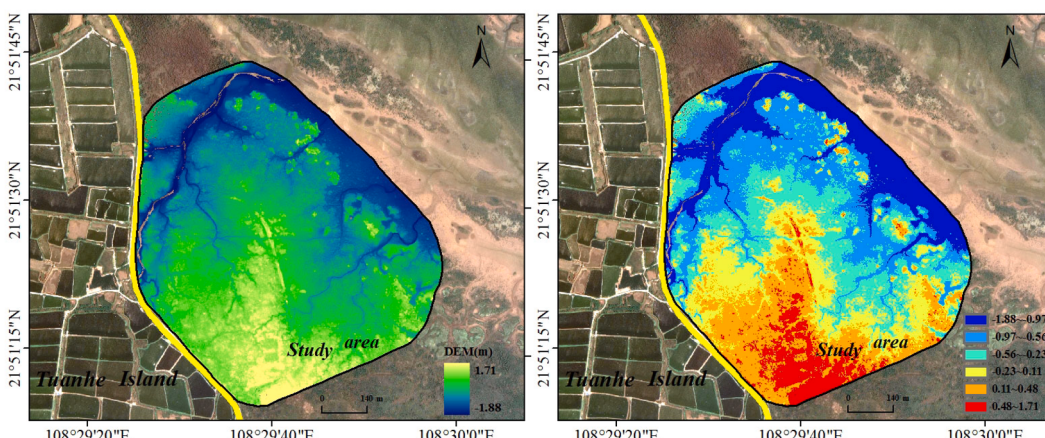


Fig. 12. Spatial distribution of DEM, and its hierarchical spatial distribution calculated.

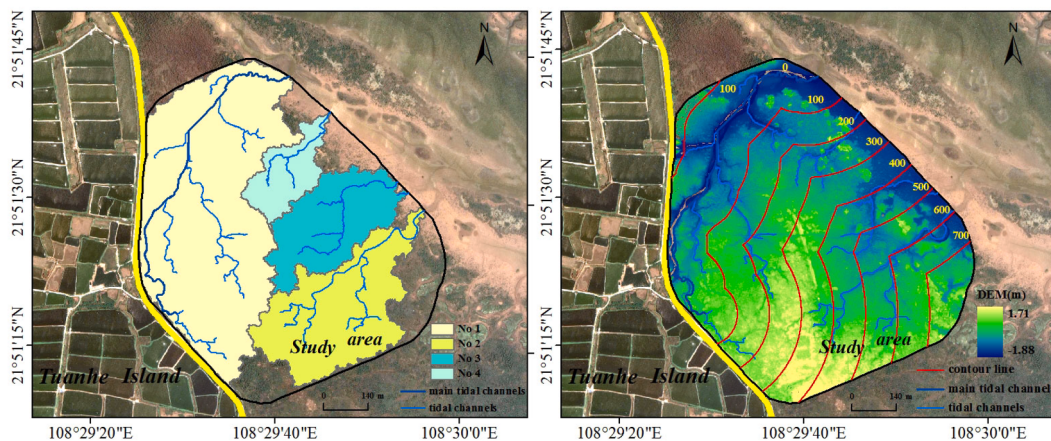


Fig. 14. Spatial distribution of subbasin in the study area, and spatial distribution of distance contour lines from main tidal channel.

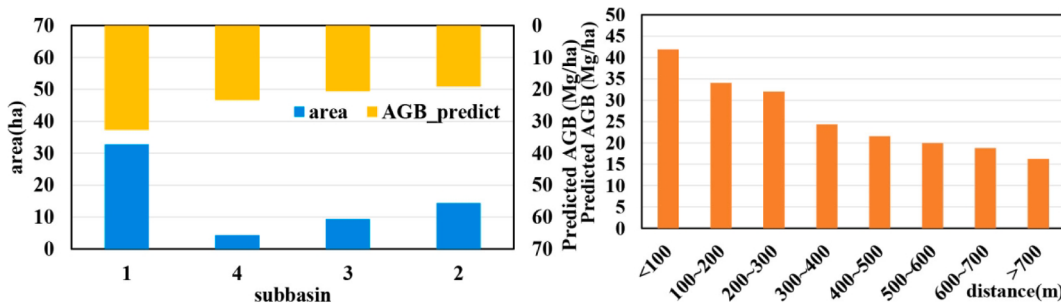


Fig. 15. Histogram of predicted biomass of mangrove in subbasin, and spatial distribution of AGB of mangroves at different distances from tidal channels.

UAV have lower cost and higher mobility than traditional manned aviation and satellite laser ICESat/GLAS data. For example, Liu et al. (2018) proved that UAV-LiDAR obtains good results in the inversion of forest structure and functional parameters. Based on 35 laser point cloud height variables and 26 laser point cloud intensity variables extracted by UAV-LiDAR, this study used the CBR machine learning model to test the fitting effect of four different variable combinations of LHI, LII, of and AI. A total of 35 height variables and 26 intensity variables were used to train the model on the basis of the results. The fitting effect of the two models was less than that of the AI model. This finding shows that the combination of height and intensity variables of the laser point cloud can improve the prediction ability of the model, which is consistent with the estimation results of mangrove aboveground biomass by Wang et al. (2020). These authors extracted 24 laser point cloud height variables and 12 intensity variables, and estimated the aboveground biomass of mangroves on Hainan Island in combination with the canopy volume index. They argued that the intensity and height variables of coupled laser point clouds often obtained higher results.

In mangrove variable importance selection, the research results of variable importance in this study show that, among the first 10 variables selected, the contribution of height variable to the model is 6, while the contribution of intensity variable to the model is only 4. Among the results of the first 38 variables whose cumulative variable importance reaches 95%, the contribution rate of the height variable is as high as 22, while the contribution of the intensity variable is only 16. Therefore, the height variable plays a major role in the contribution of *Sonneratia apetala* biomass. This may be related to the following two factors: first, the tree height of *Sonneratia apetala* in the diffusion area exhibits spatial differentiation. Fig. 11 shows that the mangrove tree height and biomass near the main tidal ditch are generally high, while the tree height in the eastern area far from the tidal ditch is small. Although *Sonneratia apetala* in the study area is diffused from artificially planted mangrove trees in the north, the height parameter of the laser point cloud is particularly

important in predicting AGB because the range of canopy height changes more. This deduction has been proven in previous studies (Otero et al., 2018). Second, this study estimated the aboveground biomass of mangroves based on the measured data, and the measured quadrat data were used to calculate the biomass on the quadrat scale according to the allometric growth equation. An important variable required in the allometric growth equation is the canopy height information, which can be easily reflected by the height variable information of the LiDAR point cloud.

4.2. Selection of machine learning model

The spatial distribution of AGB of mangroves in the study area was obtained on the basis of the intensity and height variables generated by the UAV laser point cloud and using four machine learning algorithms. Machine learning has been proven to have some advantages over traditional linear statistical regression methods for mangrove AGB estimation. These algorithms can overcome the problem of multicollinearity (Zhao et al., 2019), and these methods do not require data to obey certain distribution characteristics. However, the choice of different machine learning methods and model parameters plays a vital role in the prediction ability of the model. Many scholars use RF and SVR algorithms to estimate forest biomass, but RF is insensitive to the abnormal value of the sample. The RF classifier with the optimal hyperparametric value may overfit the training data and deviate from the prediction results (Xie et al. 2018). The boosting algorithm is sensitive to the outliers. It can flexibly process various types of data. Under relatively less parameter adjustment time, the prediction accuracy is high (Pham et al., 2020a; Pham et al., 2020b). Therefore, four boosting machine learning algorithms were selected to retrieve the biomass of the invasive *Sonneratia apetala*. The inversion results show that the inversion ability of the CBR model is the strongest. In the testing phase, R^2 is 0.7644 and the RMSE is 11.1725 Mg/ha. The second is the XGBR and

ABR models, with RMSE of 13.1052 and 13.6533 Mg/ha, respectively. Meanwhile, the fitting effect of the LGBR model is poor, with an RMSE of 18.5510 Mg/ha. Table 8 shows the 38 preferred characteristic variables used to test the accuracy of the four machine learning models: XGBR, CBR, LGBR, and ABR. In the results of the testing phase, CBR shows excellent fitting results, which indicates that the fitting ability of the model is enhanced after optimising the height and strength variables. These results are consistent with recently published findings (Wang et al., 2020; Pham et al., 2020a; Pham et al., 2020b; Dev and Eden, 2019). From the literature, we can find that XGBR, CBR, LGBR, and ABR are classic state-of-the-art boosting algorithms, which can be classified as a series of gradient lifting decision tree algorithms. These models are integrated machine-learning algorithms supported by a decision tree. XGBR is an improvement of the original GBDT algorithm, adaptive boosting is an adaptive lifting method, and LGBR and CBR are further optimised on the basis of XGBR. Compared with XGBR, LGBR and CBR have certain advantages in terms of accuracy and speed. CBR has certain advantages in dealing with feature variables, and it realises the efficient processing of category features through feature coding methods such as target variable statistics (Wang et al., 2020; Dev and Eden, 2019). In summary, the CBR machine learning method is obviously better than the other algorithms in the diffusion area of *Sonneratia apetala*. This algorithm can be used to estimate the aboveground biomass of *Sonneratia apetala* in the diffusion area in the future. In addition, a large number of parameters need to be manually set in advance in machine learning, and the process of manually adjusting the parameters of super parameters is more troublesome. A grid search method was used in this study. The anytime search method and Bayesian optimisation algorithm are also good machine parameter adjustment algorithms, which can be adjusted in the machine learning model.

4.3. Spatial distribution of mangroves and its influencing factors

Mangrove is a halophyte community growing on argillaceous swamps in estuaries of tropical and subtropical bays. It is generally distributed in the intertidal zone between the average tide level line and the average spring tide high tide level line (Liu et al., 2012; Nybakken, 1982). Although mangroves can withstand periodic seawater flooding to a certain extent, the growth of mangroves cannot exceed the 'zero boundary' (Lin, 1997) otherwise, mangroves will face the threat of death. In addition, the elevation of mangrove plants on tidal flats directly affects the time or frequency of flooding. This special environment also controls the community structure of mangrove plants and affects the aboveground biomass of mangroves. Our research results show that the biomass of *Sonneratia apetala* in the elevation zone of -0.97 m to 0.56 m presents the maximum value, and the estimation results of biomass of mangroves lower than -0.97 m show a downward trend due to long-term flooding and slow growth. This finding is consistent with Wang et al.'s (2021) view that the growth of *Aegiceras corniculata* in the Nanliujiang Estuary is affected by beach elevation. Wang et al. (2021) considered that the rapid expansion of the *Aegiceras corniculata* tree to the sea from northwest to southeast at the mouth of the Nanliujiang River is consistent with the predevelopment of tidal flat deposition to the sea, and the rise of tidal flat level becomes the key factor affecting the growth of the *A. corniculata* tree. A threshold of 0.07 m exists at the limit position suitable for the growth of *Aegiceras corniculata* seedlings. If it is lower than this threshold, the mangrove will not continue to expand. In fact, the research results of Liu et al. (2012) in Fangchenggang, Guangxi show that a large area of mangrove is located on the beach below the average sea level, of which 30% of *Aegiceras corniculata* trees in Shijiao are below the average sea level, and 56.7% of *Aegiceras corniculata* trees in Jiaodong are below the average sea level, which is consistent with the results of this study; however, it is very different from Zhang's assertion that mangroves can only grow above the average sea level (Zhang et al., 1997). In this study, *Aegiceras corniculata* has high biomass in -0.97 m to 0.56 m , but mangroves not only

can be distributed below the average sea level but also can grow well. For example, mangroves of a certain scale will also be developed in beaches below the local average sea level in some bays with good wind and wave shelter conditions (Fan, 2002; Wen, 1999).

Tidal gullies are an important component of mangrove biogeography and are important for water and sediment transport and beach migration in the intertidal zone (Wolanski et al., 1980). Biological vegetation geomorphic interactions play a key role in the control of landscape evolution. Maanen et al. (2015) constructed a dynamic model of sandy mangrove eco-geomorphology and found that mangroves can promote the formation and branching of tidal gullies, and the spatial morphology and distribution characteristics of tidal gullies also affect the development process of mangroves. Wang et al. (2018) studied the relationship between the salt marsh tidal channel and landform. They argued that the average suspended sediment flux in the intertidal zone changes from net transport to land to strong transport to the bay with an increase in tidal energy in the tidal channel. The sustainable development of tidal channels and beach landforms can promote the health of tidal flat systems. The above mentioned scholars mainly focused on the relationship between tidal gullies and biological landforms, but they do not quantitatively reveal the effect of the distribution of tidal gullies on the spatial differentiation of mangrove biomass. The results of this study show that the biomass of *Aegiceras corniculata* is related to the distance from the main tidal ditch and is unrelated to the size of the hydrological response unit. This is because the tidal ditch promotes the exchange of material and energy between the tidal beach and the external sea area through the rise and fall of the tide (Vandenbruwaene et al., 2012). More vigorous development of tidal ditches is more conducive to promoting the circulation of nutrients and biological reproduction (Teal, 1962). Using the tidal flat digital ground model, this study reveals the effects of different hydrological response units and tidal ditch distance on the biomass of *Aegiceras corniculata*, which provides a new idea for the study of the relationship between mangrove geomorphic processes and biomass.

4.4. Uncertainty of model evaluation results and future research direction

The estimation results of CBR model show that the predicted value of mangrove AGB is between 7.31 and 114.04 Mg/ha , with an average value of 25.57 Mg/ha , which is lower than the estimation result of mangrove AGB in coastal areas of Guangxi (54.40 Mg/ha) (Cao et al., 2010). However, the AGB of *Aegiceras corniculata* within 100 m near the tidal ditch is relatively high, and its AGB is mostly more than 100 Mg/ha . The vegetation carbon density of the population and community is mainly affected by planting density, survival rate, human disturbance, canopy density, age, and invasive species. Even if the same tree species is located in the same place, the biomass survey results are very different, which is related to the specific location and method of investigating the community (Li et al., 1998). The succession law of the beach mangrove community posits that a shorter succession time of the same tree species means a younger age of the community (Li et al., 1998; Liang and Wang, 2002; Cao et al., 2010), which is consistent with the view of this study. The results of this study indicate that the biomass shows a decreasing trend from west to east. The biomass of the *Sonneratia apetala* community at the edge of the tidal beach and bund in the northeast is the smallest, and its value is mostly below 10 Mg/ha . In the mangrove plant distribution area at the same latitude, climate conditions (e.g. precipitation and temperature) may also be quite different, which may affect plant biomass and its distribution pattern (Khan et al., 2009). Therefore, the evaluation results of the model are affected not only by the machine learning algorithm, but also by external factors such as precipitation and temperature. Therefore, in future studies on mangrove vegetation biomass, we should further consider the impact of different factors such as precipitation and temperature on mangroves and incorporate precipitation and temperature into mangrove biomass assessment to improve the accuracy of the model. In fact, at medium and small scales,

the biomass of *Sonneratia apetala* is affected not only by climate factors but also by soil, landform, hydrological conditions, and other factors (Hu et al., 2019). Therefore, the differences in environmental conditions in the medium and small scales should be considered in future research to further improve the accuracy of biomass estimation results.

5. Conclusions

Based on the height and intensity variables of the UAV laser point cloud, four different machine learning algorithms, namely, XGBR, CBR, LGBR, and ABR, were used to estimate the biomass of the invasive mangrove. The quantitative relationship between invasive mangrove biomass, the hydrological unit, and landform was analysed. The results are discussed as follows.

(1) The average tree height and DBH (1.3 m) of *Sonneratia apetala* are 8.23 and 15.52 cm,

respectively, which are lower than those of *Sonneratia apetala* planted in the north.

(2) The CBR model has the highest accuracy in estimating mangrove AGB ($R^2 = 0.7644$, RMSE = 11.1725 Mg/ha in the testing phase), followed by the XGBR model takes the second place ($R^2 = 0.6759$, 13.1053 Mg/ha in the testing phase), whereas the LGBR model ($R^2 = 0.3506$, RMSE = 18.5510 Mg/ha in the testing phase) has a poor fitting effect.

(3) The AGB retrieved by the CBR model shows a spatial distribution pattern of high in the northwest and low in the southeast. The values range from 7.31 Mg/ha to 114.04 Mg/ha, with an average value of 25.57 Mg/ha.

(4) The AGB of the invasive mangrove is unrelated to the area of the hydrological response unit, and its AGB is related to beach elevation and the distance of the tidal ditch. The AGB of *Sonneratia apetala* in the elevation zone of -0.97 m to 0.56 m is the largest, with a value of 28.97 Mg/ha. Above or below this elevation, biomass shows a downward trend. The AGB of *Sonneratia apetala* is lower when the distance is far from the main tidal channel. The AGB of the *Sonneratia apetala* community at the edge of the tidal band in the northeast is the smallest, and its value is mostly below 10 Mg/ha.

Declaration of Competing Interest

The authors declare that they have no known competing financial interests or personal relationships that could have appeared to influence the work reported in this paper.

Acknowledgments

This work is supported by the National Natural Science Foundation of China (Grant No. 42061020), Natural Science Foundation of Guangxi Zhuang Autonomous Region (Grant No. 2018JJA150135), Guangxi Key Research and Development Program (Grant No. AA18118038), Science and Technology Department of Guangxi Zhuang Autonomous (Grant No. 2019AC20088), the National Natural Science Key Foundation of China (Grant No. 41930537), Key Projects of Science and Technology of Guangxi Province (Grant No. AB21076016), High level talent introduction project of Beibu Gulf University (Grant No. 2019KYQD28).

References

- Alongi, D.M., 2014. Carbon cycling and storage in mangrove forests. *Annu. Rev. Mar. Sci.* 6 (1), 195–219.
- Arnold, J.G., Srinivasan, R., Muttiah, R.S., Williams, J.R., 1998. Large area hydrologic modeling and assessment part i: model development. *J. Am. Water Resour. As.* 34 (1), 73–89.
- Bouillon, S., Borges, A.V., Castañeda-Moya, E., Diele, K., Dittmar, T., Duke, N.C., Kristensen, E., Lee, S.Y., Marchand, C., Middelburg, J.J., Rivera-Monroy, V.H., Smith, T.J., Twilley, R.R., 2008. Mangrove production and carbon sinks: A revision of global budget estimates. *Global Biogeochemical Cy.* 22 (2), n/a-n/a.
- Cahyaningrum, S.T., Hartoko, A., Suryanti, 2014. Biomassa Karbon Mangrove pada Kawasan Mangrove Pulau Kemujan Taman Nasional Karimunjawa. *Diponegoro. J. Maquars*. 3 (3), 34–42.
- Cao, Q.X., Xu, D.P., Ju, H.B., 2010. The biomass estimation of mangrove community based on the textural features and spectral information of TM images. *For. Ecol. Manag.* 12 (6), 102–107.
- Castillo, J.A.A., Apan, A.A., Maraseni, T.N., Salmo, S.G., 2017. Estimation and mapping of above-ground biomass of mangrove forests and their replacement land uses in the Philippines using Sentinel imagery. *ISPRS J. Photogramm.* 134, 70–85.
- Chen, T., Guestrin, C., 2016. Xgboost: a scalable tree boosting system. In: Proceedings of the 22nd ACM SIGKDD International Conference on Knowledge Discovery and Data Mining, San Francisco, CA, USA, 13–17 August. 785–794.
- Dalla Corte, A.P., Rex, F.E., Almeida, D.R.A.d., Sanquette, C.R., Silva, C.A., Moura, M.M., Wilkinson, B., Zambrano, A.M.A., Cunha Neto, E.M.d., Veras, H.F.P., Moraes, A.d., Klauber, C., Mohan, M., Cardil, A., Broadbent, E.N., 2020. Measuring individual tree diameter and height using GatorEye High-Density UAV-lidar in an integrated crop-livestock-forest system. *Remote Sens.* 12 (5), 863. <https://doi.org/10.3390/rs12050863>.
- Deng, Y., 2020. A preliminary exploration on the ecological invasion of *Sonneratia apetala* in Qinzhou Area of Guangxi. *Hubei Forestry Sci. Technol.* 49 (5), 46–52.
- Dev, V.A., Eden, M.R., 2019. Formation lithology classification using scalable gradient boosted decision trees. *Comput. Chem. Eng.* 128, 392–404.
- Dong, L., Qingsong, G., Wenjiang, H., Den, B., Flier, J., Coolsa, A.M., 2013. Remote sensing inversion of leaf area index based on support vector machine regression in winter wheat. *Trans. Chin. Soc. Agric. Eng.* 29 (7), 117–123.
- Dorogush, A.V., Ershov, V., Gulin, A., 2018. CatBoost: gradient boosting with categorical features support [EB/OL]. arXiv. 1810, 11363.
- Fan, H.Q., 2002. *Coastal Guarder-Mangrove 145–148*, 32–36.
- Fatoyinbo, T., Feliciano, E.A., Lagomasino, D., Lee, S.K., Trettin, C., 2018. Estimating mangrove aboveground biomass from airborne lidar data: a case study from the zambezi river delta. *Environ. Res. Lett.* 13 (2), 025012. <https://doi.org/10.1088/1748-9326/aa9f03>.
- Feliciano, E.A., Shimon, W., Potts, M.D., Seung-Kuk, L., Fatoyinbo, T.E., 2017. Estimating mangrove canopy height and above-ground biomass in the everglades national park with airborne lidar and tandem-x data. *Remote Sens.* 9 (7), 702.
- Friedman, J.H., 2001. Greedy function approximation: a gradient boosting machine. *Ann. Stat.* 29, 1189–1232.
- Gao, J., 1999. A comparative study on spatial and spectral resolutions of satellite data in mapping mangrove forests. *Int. J. Remote Sens.* 20 (14), 2823–2833.
- García, M., Riaño, D., Chuvieco, E., Danson, F.M., 2010. Estimating biomass carbon stocks for a Mediterranean forest in central Spain using LiDAR height and intensity data. *Remote Sens. Environ.* 114 (4), 816–830.
- Guo, Q., Su, Y., Hu, T., Zhao, X., Wu, F., Li, Y., Liu, J., Chen, L., Xu, G., Lin, G., Zheng, Y. i., Lin, Y., Mi, X., Fei, L., Wang, X., 2017. An integrated UAV-borne lidar system for 3D habitat mapping in three forest ecosystems across China. *Int. J. Remote Sens.* 38 (8–10), 2954–2972.
- Guo, Y., Liao, J., Shen, G., 2021. Mapping large-scale mangroves along the maritime silk road from 1990 to 2015 using a novel deep learning model and landsat data. *Remote Sens.* 13 (2), 245.
- Hamdan, O., Khalil Aziz, H., Mohd Hasnadi, I., 2014. L-band ALOS PALSAR for biomass estimation of Matang Mangroves. *Malaysia. Remote Sens. Environ.* 155, 69–78.
- Hickey, S.M., Callow, N.J., Phinn, S., Lovelock, C.E., Duarte, C.M., 2018. Spatial complexities in aboveground carbon stocks of a semi-arid mangrove community: a remote sensing height-biomass-carbon approach. *Estuar. Coast. Shelf S.* 200, 194–201.
- Hirata, Y., Tabuchi, R., Patanaponpaiboon, P., Poungparn, S., Yoneda, R., Fujioka, Y., 2014. Estimation of aboveground biomass in mangrove forests using high-resolution satellite data. *J. Dent. Res.* 19 (1), 34–41.
- Howard, J., Sutton-Grier, A., Herr, D., Kleypas, J., Landis, E., Mcleod, E., Pidgeon, E., Simpson, S., 2017. Clarifying the role of coastal and marine systems in climate mitigation. *Front. Ecol. Environ.* 15 (1), 42–50.
- Hu, D.C., Zhao, H.B., 2005. Preliminary appraisal to construction benefit from multi-functional protection forest project. *Hubei Forestry Sci. Technol.* 03 (3), 20–23.
- Hu, W., Wang, Y., Zhang, D., Yu, W., Chen, G., Xie, T., Liu, Z., Ma, Z., Du, J., Chao, B., Lei, G., Chen, B., 2020. Mapping the potential of mangrove forest restoration based on species distribution models: a case study in China. *Sci. Total Environ.* 748, 142321.
- Hu, Y.K., Xu, Y.W., Xue, C.Q., Luo, Y., Liao, B.W., Zhu, N.H., 2019. Studies on carbon storages of *Sonneratia apetala* forest vegetation and soil in Guangdong province. *J. South China Agr. Univ.* 40 (6), 95–103.
- Huang, H., Liu, C., Wang, X., Zhou, X., Gong, 2018. Integration of multi-resource remotely sensed data and allometric models for forest aboveground biomass estimation in China. *Remote Sens. Environ.* 221, 225–234.
- Ibrahim, N.A., Mustapha, M.A., Lihan, T., Mazlan, A.G., 2015. Mapping mangrove changes in the Matang Mangrove Forest using multi temporal satellite imageries. *Ocean Coastal Manage.* 114, 64–76.
- Jachowski, N.R.A., Quak, M.S.Y., Friess, D.A., Duangnamon, D., Webb, E.L., Ziegler, A. D., 2013. Mangrove biomass estimation in southwest Thailand using machine learning. *Appl. Geogr.* 45, 311–321.
- Jayanthi, M., Thirumurthy, S., Nagaraj, G., Muralidhar, M., Ravichandran, P., 2018. Spatial and temporal changes in mangrove cover across the protected and unprotected forests of India. *Estuar. Coast. Shelf Sci.* 213, 81–91.
- Jian, Q., Chen, Hsin, Y., Wen, Jie, Dai, W.J., Lv, Yu-Chian, C., 2019. Artificial intelligence approach to find lead compounds for treating tumors. *J. Phys. Chem. Lett.* 10 (15), 4382–4400.

- Khan, M., Suwa, R., Hagihara, A., 2009. Biomass and aboveground net primary production in a subtropical mangrove stand of *Kandelia obovata* (S. L.) Yong at Manko Wetland, Okinawa, Japan. *Wetl. Ecol. Manag.* 17(6), 585–599.
- Kovacs, J.M., Zhang, C., Flores-Verdugo, F.J., 2008. Mapping the condition of mangroves of the Mexican Pacific using C-band ENVISAT ASAR and Landsat optical data. *Cienc. Mar.* 34, 407–418.
- Le, H.T., Tran, T.V., Gyeitshen, S., Nguyen, C.P.T., Tran, D.X., Luu, T.H., Duong, M.B., 2020. Characterizing spatiotemporal patterns of Mangrove forests in Can Gio biosphere reserve using sentinel-2 imagery. *Appl. Sci. Basel.* 10, 17.
- Li, T., 2020. Research application of point cloud filtering algorithm based on cloth simulation in railway airborne LiDAR. *Railway Invest. Surv.* 46 (5), 13–17.
- Li, Y., Zheng, D., Chen, H., Liao, B., Deng, S., Chen, X., 1998. Preliminary study on introduction of mangrove *Sonneratia apetala* buch-ham. *For. Res.* 11 (1), 39–44.
- Liao, J.J., Zhen, J.N., Zhang, L., Metternicht, G., 2019. Understanding dynamics of mangrove forest on protected areas of Hainan Island, China: 30 years of evidence from remote sensing. *Sustainability* 11, 16.
- Liang, S.C., Wang, B., 2002. Fractal characteristics of population canopy structure of the mangrove species, *Bruguiera gymnorhiza*. *J. Mar. Sci. Bull.* 21 (5), 26–31.
- Lin, G., Fu, J.Y., Jiang, D., Wang, J.H., Wang, Q., Dong, D.L., 2015. Spatial variation of the relationship between pm2.5 concentrations and meteorological parameters in china. *Biomed. Res. Int.* 29, 1–15.
- Lin, P., 1997. Mangrove Ecosystem in China. Science Press, Beijing, pp. 85–91.
- Liu, K., Shen, X., Cao, L., Wang, G., Cao, F., 2018. Estimating forest structural attributes using UAV-LiDAR data in Ginkgo plantations. *ISPRS J Photogramm.* 146, 465–482.
- Liu, H., Ren, H., Hui, D., Wang, W., Liao, B., Cao, Q., 2014. Carbon stocks and potential carbon storage in the mangrove forests of China. *J. Environ. Manage.* 133, 86–93.
- Liu, L., Fan, H.Q., Li, C.G., 2012. Tide elevations for four mangrove species along western coast of Guangxi, China. *Acta Ecol. Sin.* 32 (3), 690–698.
- Lu, D., Chen, Q., Wang, G., Liu, L., Li, G., Moran, E., 2014. A survey of remote sensing-based aboveground biomass estimation methods in forest ecosystems. *Int. J. Digit. Earth.* 09, 63–105.
- Lu, D.S., 2006. The potential and challenge of remote sensing-based biomass estimation. *Int. J. Remote Sens.* 27 (7), 1297–1328.
- Luo, S., Chui, T.F.M., 2020. Annual variations in regional mangrove cover in southern China and potential macro-climatic and hydrological indicators. *Ecol. Ind.* 110, 105927.
- Maanen, B.V., Coco, G., Bryan, K.R., 2015. On the ecogeomorphological feedbacks that control tidal channel network evolution in a sandy mangrove setting. *P. Roy. Soc. A.* 471 (2180), 20150115.
- MacDonnell, C.P., Zhang, L., Griffiths, L., Mitsch, W.J., 2017. Nutrient concentrations in tidal creeks as indicators of the water quality role of mangrove wetlands in Southwest Florida. *Ecol. Ind.* 80, 316–326.
- Manna, S., Nandy, S., Chanda, A., Akhand, A., Hazra, S., Dadhwal, V.K., 2014. Estimating aboveground biomass in *Avicennia marina* plantation in Indian Sundarbans using high-resolution satellite data. *J. Appl. Remote Sens.* 28, 083638.
- McLeod, E., Chmura, G.L., Bouillon, S., Salm, R., Björk, M., Duarte, M.C., Lovelock, C.E., Schlesinger, W.H., Silliman, B.R., 2011. A blueprint for blue carbon: toward an improved understanding of the role of vegetated coastal habitats in sequestering CO₂. *Front. Ecol. Environ.* 9 (10), 552–560.
- Mumby, P.J., Edwards, A.J., Arias-Gonzalez, J.E., Lindeman, K.C., Blackwell, P.G., Gall, A., Gorczynska, M.I., Harborne, A.R., Pescod, C.L., Renken, H., 2004. Mangroves enhance the biomass of coral reef fish communities in the Caribbean. *Nature* 427, 533–536.
- Murdiyarso, D., Purbopuspito, J., Kauffman, J.B., Warren, M.W., Sasmito, S.D., Donato, D.C., Manuri, S., Krisnawati, H., Taberima, S., Kurnianto, S., 2015. The potential of Indonesian mangrove forests for global climate change mitigation. *Nat. Clim. Change.* 5 (12), 1089–1092.
- Nbakken, J.W., 1982. Marine Biology-An Ecological Approach. Harper and Row Publishers, New York, pp. 260–280.
- Navarro, J.A., Algeit, N., Fernández-Landa, A., Esteban, J., Rodríguez-Noriega, P., Guillén-Climent, M.L., 2019. Integration of UAV, Sentinel-1, and Sentinel-2 data for mangrove plantation aboveground biomass monitoring in Senegal. *Remote Sens.* 11, 77.
- Otero, V., Van De Kerchove, R., Satyanarayana, B., Martínez-Espinosa, C., Fisol, M.A.B., Ibrahim, M.R.B., Sulong, I., Mohd-Lokman, H., Lucas, R., Dahdouh-Guebas, F., 2018. Managing mangrove forests from the sky: forest inventory using field data and unmanned aerial vehicle (UAV) imagery in the Matang mangrove forest reserve, peninsular Malaysia. *For. Ecol. Manag.* 411, 35–45.
- Pandit, S., Tsuyuki, S., Dube, T., 2018. Landscape-scale aboveground biomass estimation in buffer zone community forests of central Nepal: coupling in situ measurements with Landsat 8 satellite data. *Remote Sens.* 10.
- Peng, L., Liu, K., Cao, J., Zhu, Y., Liu, L., 2019. Combining GF-2 and Rapideye satellite data for mapping mangrove species using ensemble machine-learning methods. *Int. J. Remote Sens.* 41 (3), 1–26.
- Pham, L.T.H., Brabyn, L., 2017. Monitoring mangrove biomass change in Vietnam using spot images and an object-based approach combined with machine learning algorithms. *ISPRS J. Photogramm.* 128, 86–97.
- Pham, T.D., Le, N.N., Ha, N.T., Nguyen, L.V., Xia, J., Yokoya, N., To, T.T., Trinh, H.X., Kieu, L.Q., Takeuchi, W., 2020a. Estimating mangrove above-ground biomass using extreme gradient boosting decision trees algorithm with fused Sentinel-2 and ALOS-2 PALSAR-2 data in can gio biosphere reserve. Vietnam. *Int. Remote Sens.* 12, 777.
- Pham, T.D., Yokoya, N., Bui, D.T., Yoshino, K., Friess, D.A., 2019. Remote sensing approaches for monitoring mangrove species, structure, and biomass: opportunities and challenges. *Remote Sens.* 11 (3), 230.
- Pham, T.D., Yokoya, N., Xia, J., Ha, N.T., Le, N.N., Nguyen, T.T.T., Dao, T.H., Vu, T.T.P., Pham, T.D., Takeuchi, W., 2020b. Comparison of machine learning methods for estimating mangrove above-ground biomass using multiple source remote sensing data in the Red River Delta biosphere reserve. Vietnam. *Remote Sens.* 12, 1334.
- Pham, T.D., Yoshino, K., Le, N., Bui, D., 2018. Estimating aboveground biomass of a mangrove plantation on the northern coast of Vietnam using machine learning techniques with an integration of alos-2 palsar-2 and sentinel-2a data. *Int. J. Remote Sens.* 39, 7761–7788.
- Phua, M.H., Ling, Z.Y., Wong, W., Korom, A., Takao, G., 2014. Estimation of above-ground biomass of a tropical forest in northern borneo using high-resolution satellite image. *J. Forest Environ. Sci.* 30 (2), 233–242.
- Qiu, P.H., Wang, D.Z., Zuo, X.Q., Yang, X., Xie, G.Z., Xu, S.J., Zhong, Z.Q., 2019. Finer resolution estimation and mapping of mangrove biomass using UAV LiDAR and WorldView-2 Data. *Remote Sens.* 10 (10), 871.
- Sadeghi, S.H., Dashpadergi, M.M., Rekabdarkoolai, H.M., Schoorl, J.M., 2021. Sensitivity analysis of relationships between hydrograph components and landscapes metrics extracted from digital elevation models with different spatial resolutions. *Ecol. Ind.* 121, 107025.
- Salum, R.B., Souza-Filho, P., Simard, M., Simard, M., Silva, C.A., Fernandes, M., Cougo, M., Junior, W., Rogers, K., 2020. Improving mangrove above-ground biomass estimates using LiDAR. *Estuar. Coast. Shelf S.* 236, 106585.
- Shi, Y.F., Wang, T.J., Skidmore, A.K., Heurich, M., 2018. Important LiDAR metrics for discriminating forest tree species in Central Europe. *ISPRS J. Photogramm.* 137, 163–174.
- Soares, M.L.G., Schaeffer-Novelli, Y., 2005. Above-ground biomass of mangrove species. I. Analysis of models. *Estuar. Coast Shelf S.* 2005, 65(1/2):1–18.
- Song, K., Yan, F., Ding, T., Gao, L., Lu, S., 2020. A steel property optimization model based on the XGBoost algorithm and improved PSO. *Comp. Mater. Sci.* 174, 109472.
- Song, K.S., Zhang, B., Wang, Z.M., Zhang, Y.Z., Liu, H.J., 2006. Soybean LAI estimation with in-situ collected hyperspectral data based on BP-neural networks. *Sci. Agric. Sin.* 39 (6), 1138–1145.
- Tang, Y.J., Fang, Z.Q., Zhong, Y.T., Zhang, Z.W., Chen, K., An, D., Yang, X.B., Liao, B.W., 2012. Succession of macrofauna communities in wetlands of Sonneratia apetala artificial mangroves during different ecological restoration stages. *Acta Ecol. Sin.* 32 (10), 3160–3169.
- Teal, J.M., 1962. Energy flow in the salt marsh ecosystem of Georgia. *Ecology* 43 (4), 614–624.
- Tian, Y., Huang, H., Zhou, G., Zhang, Y., Tao, J., Zhang, Y., Lin, J., 2021. Aboveground mangrove biomass estimation in Beibu Gulf using machine learning and UAV remote sensing. *Sci. Total Environ.* 781, 146816.
- Tian, Y.C., Huang, Y.L., Zhang, Q., Zhang, Y.L., Huang, H., Liang, M.Z., Zhou, G.Q., 2019. A comparative study of spatial heterogeneity of ecosystem service value in typical islands in Beibu Gulf. *Mar. Sci.* 43 (2), 60–68.
- Trégarot, E., Caillaud, A., Cornet, C.C., Taureau, F., Catry, T., Cragg, S., Failler, P., 2021. Mangrove ecological services at the forefront of coastal change in the French overseas territories. *Sci. Total Environ.* 763, 143004.
- Vaghela, B., Chirakkal, S., Putrevu, D., Solanki, A.D., 2021. Modelling above ground biomass of Indian mangrove forest using dual-pol SAR data. *Remote Sens. Appl.: Soc. Environ.* 21, 100457.
- Vandenbruwaene, W., Meire, P., Temmerman, S., 2012. Formation and evolution of a tidal channel network within a constructed tidal marsh. *Geomorphology* 151, 114–125.
- Wang, D.Z., Wan, B., Liu, J., Su, Y.J., Guo, Q.H., Qiu, P.H., Wu, X.C., 2020. Estimating aboveground biomass of the mangrove forests on northeast Hainan Island in China using an upscaling method from field plots, UAV-LiDAR data and Sentinel-2 imagery. *Int. J. Appl. Earth. Obs.* 85, 101986.
- Wang, D.Z., Wan, B., Qiu, P.H., Zuo, Z.J., Wang, R., Wu, X.C., 2019a. Mapping height and aboveground biomass of mangrove forests on Hainan Island Using UAV-LiDAR sampling. *Remote Sens.* 11 (18), 2156.
- Wang, L., Jia, M., Yin, D., Tian, J., 2019b. A review of remote sensing for mangrove forests: 1956–2018. *Remote Sens. Environ.* 231, 111223.
- Wang, R., Dai, Z., Huang, H., Long, C., Liang, X., Li, S., 2021. Research on biomorphodynamics processes of *Aegiceras corniculatum* in the Nanliu River estuary. *Acta Oceanol. Sin.* 43 (9), 102–114.
- Wang, X., Hu, M., Ren, H., Li, J., Tong, C., Musenze, R.S., 2018. Seasonal variations of nitrous oxide fluxes and soil denitrification rates in subtropical freshwater and brackish tidal marshes of the Min River estuary. *Sci. Total Environ.* 616, 1404–1413.
- Wen, Y., 1999. Biomass and productivity of five mangrove communities in Yingluo Bay of Guangxi. *Guangxi Sci.* 6 (2), 142–147.
- Wicaksono, P., Danoedoro, P., Hartono, N., 2016. Mangrove biomass carbon stock mapping of the Karimunjawa Islands using multispectral remote sensing. *Int. J. Remote Sens.* 37 (1), 26–52.
- WillKoehrsen, Feature-selector, 2019, https://github.com/WillKoehrsen/featureselector/blob/master/feature_selector/feature_selector.py.
- Wolanski, E., Jones, M., Bunt, J.S., 1980. Hydrodynamics of a tidal creek-mangrove swamp system. *Mar. Freshwater Res.* 31 (4), 431–450.
- Wu, C., Shen, H., Shen, A., Deng, J., Gan, M., Zhu, J., Xu, H., Wang, K., 2016. Comparison of machine-learning methods for above-ground biomass estimation based on Landsat imagery. *J. Appl. Remote Sens.* 10 (3), 035010.
- Xia, J., Du, P., He, X., Chanussot, J., 2014. Hyperspectral remote sensing image classification based on rotation forest. *IEEE Geosci. Remote S.* 11 (1), 239–243.
- Xia, Q., Jia, M.M., He, T.T., Xing, X.M., Zhu, L.J., 2021. Effect of tide level on submerged mangrove recognition index using multi-temporal remotely-sensed data. *Ecol. Ind.* 131, 108169.
- Xie, Y., Zhu, C., Zhou, W., Li, Z., Liu, X., Tu, M., 2018. Evaluation of machine learning methods for formation lithology identification: a comparison of tuning processes and model performances. *J. Pet. Sci. Eng.* 160, 182–193.

- Xu, Y., Wang, J., Xia, A., Zhang, Y., Dong, X., Wu, K., Wu, G., 2019. Continuous wavelet analysis of leaf reflectance improves classification accuracy of mangrove species. *Remote Sens.* 11 (3), 254.
- Yang, F.Q., Feng, H.K., Li, Z.H., Gao, L., Yang, G.J., Dai, H.Y., 2016. Hyperspectral estimation of leaf area index for winter wheat based on Akaike's information criterion. *Trans. Chin. Soc. Agr. Eng.* 32 (3), 163–168.
- Yees, M., 2010. Redd and Blue Carbon: Carbon Payments for Mangrove Conservation. University of Georgia, Athens.
- Yuan, Y.N., Peng, D.L., Wang, W., Zeng, W.S., 2021. Estimating standing stocks of the typical conifer stands in northeast china based on airborne lidar data. *Chin. J. Appl. Ecol.* 32 (3), 836–844.
- Zhang, H.B., Luo, Y.M., Liu, X.H., Fu, C.C., 2015. Current researches and prospects on the coastal blue carbon (in Chinese). *Sci. Sin. Terr.* 45, 1641–1648.
- Zhang, Q.M., Yu, H.B., Chen, X.S., Zheng, D.Z., 1997. The relationship between mangrove zone on tidal flats and tidal levels. *Acta. Ecol. Sin.* 17 (3), 258–265.
- Zhao, Q., Yu, S., Zhao, F., Tian, L., Zhao, Z., 2019. Comparison of machine learning algorithms for forest parameter estimations and application for forest quality assessments. *For. Ecol. Manag.* 434, 224–234.
- Zhou, B., Bartholmai, B.J., Kalra, S., Osborn, T., Zhang, X., 2021. Lung mass density prediction using machine learning based on ultrasound surface wave elastography and pulmonary function testing. *J. Acoust. Soc. Am.* 149 (2), 1318–1323.
- Zhou, L., Ma, Y.i., Ren, G., 2019a. Change analysis of mangrove in Bangladesh coastal zone based on remote sensing in the recent 30 years. *Marine. Environ Sci.* 38 (1), 60–67.
- Zhou, T., Yang, J., Zhou, Q., Tan, B., Zhou, Y., Jian, X., Sun, Y., 2019b. Power system transient stability assessment method based on modified LightGBM. *Power Syst. Technol.* 43 (6), 1931–1940.
- Zhu, B., Liao, J., Shen, G., 2021. Combining time series and land cover data for analyzing spatio-temporal changes in mangrove forests: a case study of qinglangang nature reserve, hainan, china. *Ecol. Ind.* 131, 108135.
- Zhu, Y., Liu, K., Liu, L., Wang, S., Liu, H., 2015. Retrieval of mangrove aboveground biomass at the individual species level with worldview-2 images. *Remote Sens.* 7 (9), 12192–12214.